

Analysis of Estimation Algorithms for
Autonomous Navigation with TDRSS DATA¹

By

J. Dunham, A. Long, P. Gural
K. Preiss, and H. Sielski

Computer Sciences Corporation

ABSTRACT

An investigation was performed to determine an appropriate estimation technique for onboard orbit determination using Tracking and Data Relay Satellite System (TDRSS) data. The two user satellite orbits which were studied are similar to Landsat-D (near-circular, 700-kilometers altitude, near-polar inclination). The following estimation algorithms were identified as candidates for use in autonomous navigation: (1) the extended Kalman filter (EKF) with process noise, (2) the EKF with consider parameters (CEKF), (3) the sequential Kalman filter with consider parameters (CKF), and (4) the batch least-squares differential correction technique (DC). The candidate estimators were evaluated with respect to their performance with both baseline and worst case TDRSS measurement errors and tracking configurations.

Two different modes of operation were studied. The one-way uses Doppler data which are collected on the user satellite. The two-way mode uses range and Doppler data which are collected on the ground and transmitted in the command stream to the user satellite for processing.

The actual data used in this study were simulated satellite-to-satellite range and delta range from TDRS East and West to the user, scheduled in 10-minute passes of six pairs of range/delta-range observations per minute. Various tracking frequencies were used, ranging from tracking once per orbit

¹Work performed under NASA Contract NAS 5-24300

to tracking every third orbit. Data sets of 12 or 24 hours length were generated which simulated the expected range of errors in the TDRS ephemerides, the onboard force model, and the user clock (one-way only). Transient problems were also simulated such as TDRS ephemeris updates, and passes of data with large biases or high noise.

Identical data sets were used in evaluating the estimation algorithms. The user satellite state was estimated for both modes. For the one-way mode, the onboard oscillator frequency bias was also estimated. The user ephemeris resulting from each estimation process was compared to the truth model to determine the accuracy and reliability of that estimation process was compared to the truth model to determine the accuracy and reliability of that estimation process in both baseline and worst cases. The process noise levels in the EKF were varied to determine the optimum range. The performances of the CEKF and CKF were analyzed to determine an appropriate set of consider parameters and their a priori variances. In addition, a method of automating the DC processing was evaluated.

I. INTRODUCTION

National Aeronautic and Space Administration operational support of satellite missions of the future will require the annotation of data collected onboard with ancillary data, which includes the spacecraft orbit, attitude, and time. If the spacecraft position and velocity can be determined entirely onboard, it will improve the system responsiveness by providing fully annotated payload data without the requirement for post facto processing or other ground support. Onboard data annotation will also decrease the ground support requirements for spacecraft and attitude control and instrument operations.

Toward this end, Goddard Space Flight Center (GSFC) is currently investigating the feasibility of autonomous spacecraft navigation with Tracking and Data Relay Satellite System (TDRSS) data. The use of TDRSS data for onboard estimation has the advantage that the NASA will already be using TDRSS for ground-based satellite tracking and the relay of command and telemetry data. Therefore, TDRSS interfaces will already exist, and NASA spacecraft will be equipped with TDRSS transponders. However, the major constraint in the use of TDRSS is that only a limited number of users may use the forward link over a given time span, which limits the frequency of tracking contacts.

An onboard orbit determination algorithm must be selected for use with TDRSS data that will provide both reliability and accuracy. Three estimation algorithms are being studied to determine their suitability for onboard use with TDRSS data: the extended Kalman Filter (EKF), the batch least-squares estimator, and the consider filter. The performance of these estimators was compared with respect to: 1) accuracy using a nominal tracking schedule, 2) effect of reducing the tracking schedule, 3) effect of large TDRS ephemeris errors,

and 4) accuracy in the presence of anomalous or deleted passes of data. This paper presents an overview of the results of the studies made, which are described in detail in References 1,2, and 3. The work described herein was carried out under Contract NAS 5-24300 using the capabilities of the Research and Development Goddard Trajectory Determination System (R&D GTDS) available at the time of the study (References 4, 5, and 6).

II. PROTOTYPE SYSTEM

A prototype onboard orbit determination system for use with TDRSS data is being developed by the Advanced Systems Program of the Office of Space Tracking and Data Systems (OSTDS) to demonstrate its feasibility. This work includes analysis to select a suitable estimation technique, and design and implementation of a candidate system on a LSI-11/23 microprocessor. The prototype system will be a combination of hardware and software designed to simulate the onboard operation and ground support of the orbit determination system.

Two tracking modes are being studied for use onboard, one-way Doppler and two-way range and/or Doppler. The one-way Doppler measurements are extracted onboard the user satellite from tracking signals originating on the ground, relayed through a TDRS, and received by the user spacecraft. The accuracy of the one-way measurements will be degraded by any errors in the user frequency standard that is used in extracting the Doppler measurements. The geometry of this measurement is illustrated in Figure 2-1. The two-way data are extracted on the ground from the round-trip propagation of the tracking signals; the resulting data are collected and relayed back to the user spacecraft through the communications link. The two-way measurement geometry is illustrated in Figure 2-2. Comparison of Figure 2-1 and 2-2 shows that the

one-way data is from the forward link of the round-trip measurement which produces the two-way data.

A diagram of the proposed orbit determination concept and its interaction with other satellite systems is shown in Figure 2-3 (adapted from Ref. 7). Those areas outlined by the dashed lines indicate the additional requirements for the onboard orbit determination. Both one-way and two-way data types will require additional onboard computer capability for the orbit determination. One-way navigation will require modification of the standard TDRSS transponder to permit Doppler extraction and signal acquisition.

For both navigation modes, the Payload Operations Control Center (POCC) transmits the TDRSS ephemerides via the TDRSS to the user spacecraft. For two-way tracking data, the measurements, along with accurate time tags and frequency reference provided by the standard clock at White Sands Tracking Facility (WSTF), are placed in the command stream and transmitted to the user via TDRSS. In the one-way navigation mode, the navigation computer uses the TDRSS ephemeris and the a priori satellite state estimate to predict the Doppler measurement for signal acquisition. The two-way data navigation mode can be one for estimation recovery after a user spacecraft maneuver, or any event requiring estimation initialization, and then the navigation mode switched to one-way data. Once measurements are available, they are passed to the orbit determination module for estimating the user satellite ephemeris and, for one-way data, the oscillator frequency bias. Other modeling parameters related to the effects of atmospheric drag or to the frequency standard may also be estimated. The satellite ephemeris produced by the estimation process is passed to the general purpose onboard computer for use instead of the ground-uplinked ephemeris.

III. ESTIMATORS

Four estimation techniques were selected for study; an extended Kalman filter (EKF), a sliding batch differential corrector (SBDC), a consider Kalman filter (CKF), and a consider extended Kalman filter (CEKF). The EKF was available in R&D GTDS, and the SBDC, CKF, and CEKF were made available through temporary modifications to the R&D GTDS software. These orbit determination techniques were studied to determine their reliability and accuracy in the presence of measurement errors and data problems associated with TDRSS data. Figure 3-1 lists the major characteristics of each estimator.

Extended Kalman Filter (EKF)

The R&D GTDS Filter Program (Reference 5) contains an EKF estimator with a simple process noise covariance matrix model. It was recognized that the sequential processing capability of the EKF would be advantageous for onboard orbit estimation, although the data coverage would be sparse (at most, a 10-minute pass of data per orbit), not an optimal configuration for a filter. The operational flow of an EKF is given in Figure 3-2.

In the EKF, the state, clock, and drag covariance process noise rates were modeled using the linear model

$$Q(t_k) = Q \cdot (t_k - t_{k-1})$$

where $Q(t_k)$ = process noise

\dot{Q} = diagonal matrix of constants that are the assumed noise variance rates of change for the solve-for parameter set

t_k = measurement time

t_{k-1} = measurement time of previous observation

The state covariance is augmented by $Q(t_k)$ at each measurement time, t_k . In the current study, nonzero process noise rates of change were used for the velocity, clock drift, and drag terms.

Sliding Batch Differential Correction (SBDC)

The batch least-squares estimation (DC) program of R&D GTDS, described in References 4 and 6 was modified, as described in Reference 2, to sequentially process a series of data spans through a large data set. The program starts with a span of data approximately 12 hours, with which it estimates the satellite position and velocity state, and other parameters, as requested. After converging to a solution, a new data span is created by adding new data and deleting old data. A new solution is then attempted on this data. In a typical run selecting 12 hour spans from a file covering 24 hours, five solutions and five separate DC Program runs are made.

The SBDC flow is described in Figure 3-3.

Consider Kalman Filter (CKF) and Consider Extended Kalman Filter (CEKF)

The FILTER Program of R&D GTDS, as described in Reference 5, was modified to include a consider feature, used in place of the process noise covariance matrix. The motivation for this investigation was to compare the CKF and CEKF results to those of the EKF and the SBDC to see if the consider feature, which models the estimation error in a more physically meaningful way, would perform better than the EKF or SBDC or lead to a better understanding of the estimation results from the EKF and SBDC.

The KF and EKF can be easily modified to the CKF and CEKF by setting the relevant gain terms to zero. If the state

update equation is partitioned into the solve-for (X) and consider (Z) portions, then the state update, \hat{x} , is

$$\begin{bmatrix} \hat{x} \\ \hat{z} \end{bmatrix} = \begin{bmatrix} \bar{x} \\ \bar{z} \end{bmatrix} + \begin{bmatrix} K \\ 0 \end{bmatrix} \left\{ y - \begin{bmatrix} H_x & H_z \end{bmatrix} \begin{bmatrix} \bar{x} \\ \bar{z} \end{bmatrix} \right\}$$

where H_x and H_z are the partial derivatives of the observation equation with respect to the solve and the consider parameters, respectively.

The covariance is also partitioned to be

$$P = \begin{bmatrix} P_x & P_{xz} \\ P_{zx} & P_z \end{bmatrix}$$

If the a priori cross terms P_{xz} and P_{zx} are assumed to be zero, the Kalman gain is

$$K = \bar{P}_x H_x^T \left[H_x \bar{P}_x H_x^T + H_z P_z H_z^T + R \right]^{-1}$$

$$P_x = \begin{bmatrix} I & -K H_x \end{bmatrix} \bar{P}_x$$

$$P_{xz} = -K H_z P_z$$

The propagated estimate to the error in Z, \bar{z} , will be zero, since no estimate is made of the Z error. Then the state update will be

$$\hat{x} = \bar{x} + K(y - H_x \bar{x})$$

For the CKF, the processing done until the last data point is processed, and then the state is updated

$$\hat{x}_l = x_l + \hat{x}_l$$

If the CKF has not converged, the updated state \hat{X}_l is propagated back to the first observation and the process begins again.

For the CEKF, the state update becomes:

$$\hat{X}_K = X_K + K_k y_k$$

which are then the initial conditions for integration to the next data point.

IV Evaluation Procedure

Several programs available in R&D GTDS were used in the evaluation of the orbit determination accuracy. Figure 4-1 illustrates the evaluation procedure by which the ephemeris of a "truth" model for the user satellite was compared with the ephemeris produced by the estimator. Deviations between the two ephemerides provide a measurement of the accuracy obtained by the estimator for a particular test case. The simulated data used by the estimator is supplied by the DATASIM Program, which has the capability to corrupt the range and delta-range measurements with measurement errors and random measurement noise.

The time spans for the comparisons for each estimator are chosen to cover times which correspond to those in which an operational onboard estimator would be annotating data. In the case of the CKF, and the SBDC, this is a span covering at least one orbit, and possibly two, beyond the last data points. For the EKF and the CEKF, this comparison time span is one covering an orbit or more well beyond (that is, several orbits) the initial data. This time span should be one in which the effects of initialization of the filter are not noticeable, and the filter has settled to a steady state or equilibrium condition. Since it is of some interest to learn how long this settling process takes, two comparison spans are used, one at the mid-point and one at the end of the data.

The analysis procedure used in comparing the ephemerides involved examining (1) the solve-for parameter report, (2) the root mean square (rms) and the maximum deviations of the position and velocity errors, and (3) the radial, along-track, and cross-track ephemeris comparison plots of the position and velocity errors for the full estimation time

span. These statistics were recorded for all cases, along with pass frequency, numbers of TDRSS observed, and measurement and modeling errors applied.

Test Cases

The Landsat-D and Gamma Ray Observatory, (GRO) spacecraft were selected as the sample test cases for onboard orbit estimation. Landsat-D has a near-polar inclination and a medium altitude. GRO, on the other hand, has a lower altitude and a less inclined orbit. Table 4-1 lists the Landsat-D and GRO orbital elements and spacecraft parameters. The TDRSS satellites were placed in nearly circular stationary orbits 130° apart with periods of 1436.2 minutes.

Measurement Models for TDRSS Data

For the purpose of this study, three separate data-type cases were considered for evaluation: one-way Doppler data, two-way Doppler data, and two-way range and Doppler data. The Doppler measurement was simulated as a delta-range measurement so that existing R&D GTDS capabilities could be used.

The range and delta-range measurements were simulated using the pseudo-TDRSS data capabilities in the Data Simulation (DATASIM) program of R&D GTDS. A discussion of these measurements can be found in Reference 1. A set of range and/or delta-range measurements constitute a pass of data. In all cases, it was assumed that the user satellite was in contact with a single TDRS for 10 minutes for each pass of data. The time between range and delta-range measurements and the delta-range computation interval were set at 10 seconds, which yields 30 delta-range measurements for every complete pass of data. For both measurement types combined, there are 30 range and 30 delta-range measurements.

TDRSS Tracking Schedules

The TDRSS observation simulation determines the TDRSS visibility from the user spacecraft by testing to see if the TDRSS falls within the user antenna and that it is not occulted by the Earth. The effects of atmospheric refraction are not included in the observation modeling. With an antenna modeled as a cone pointing along the radial direction with a half-angle of 100° , the time span of line-of-sight contact between Landsat-D or GRO and any single TDRS ranges from 40 to 60 minutes. During the early phases of the feasibility study, several models were run to investigate the dependence of the prediction accuracy on the time from the first or last possible contact with a TDRS. It was determined that tracking measurements made consistently at the beginning or end of a visibility interval (edge-justified data) yield better estimation accuracy than those centered in the visibility arc (center-justified data). Since neither data set represents a realistic case, a more random model was selected for use in the remainder of the study. Another variable in the tracking schedule was the length of time between subsequent passes of data. To study this, estimation was done with time gaps of one, two, or three user-satellite revolutions between data passes. For the one revolution gap, a Landsat-D data set covering a 24-hour time span will have 17 passes of data. For the same time span, a set with a two revolution gap will contain 9 passes of data, and, with a three revolution gap, 6 passes of data. For any given pass of data, the user satellite was restricted to tracking by only one TDRS. However, most models were run with alternating TDRS contacts on subsequent passes of data.

Figure 4-2 shows the TDRS visibility for the GRO satellite, and the location of the data sets used for the one revolution gap GRO studies.

Measurement Error Models And Anomalous Data

Each observation in a data set, consists of the observed quantity, range or delta-range, its time tag, and the TDRS identification and coordinates at the time of the observation. The scheduling of the observations and the delta-range integration time are supplied by the user. The R&D GTDS DATASIM Program applies biases and random errors to the measurements. Errors on the TDRS ephemeris are applied to the TDRS coordinates included in each observational record. The frequency bias is added to the delta-range observation and the user clock error is applied to the observation time tag.

The nominal values for each of these error sources are listed in Tables 4-2, 4-3 and 4-4, respectively.

To study the performances of the estimators in the presence of transitory data problems, data sets were created in which one or more ten-minute passes of data were given anomalously large errors. The operation of this data simulation technique is explained in detail in Reference 2.

The errors may include any or all of the following:

- Larger TDRS ephemeris errors in the along-track(L), cross-track(C), radial(H) and/or L components
- Larger range and/or delta-range measurement noise
- Larger bias on the range data
- Bias on the delta-range data

These errors are applied to one or more specific passes in a 24-hour data set. In this way, the effects of transitory problems which are periodic or create larger random errors or a bias on the data can be studied.

Dynamic Modeling Errors

Dynamic modeling errors are simulated by a mismatch of the

spacecraft acceleration and frequency standard that are used in the data simulation from those used in the estimation.

Physically, these errors arise from the lack of precise models for the accelerations acting on the spacecraft and the behavior of onboard clocks. The dynamic modeling errors affect the accuracy of the propagation of the orbital and clock state vectors. The dynamic models used in the truth model, and in the estimators, the EKF, the SBDC, the CKF and the CEKF, are given in Table 4-5.

Table 4-6 gives the maximum deviation in 24 hours due to the dynamic modeling differences between the truth and the estimation models for the SBDC. Figures 4-3 and 4-4 show the along-track growth of these errors over 12 hours for Landsat-D and GRO. Similar results for the EKF force model show a larger error growth.

Baseline Parameters

Table 4-7 lists the parameters that were estimated and those from which the consider parameters were chosen. Table 4-8 lists the a priori offsets or values, a priori covariances associated with the estimated parameters, and the measurement standard deviations that were used in the baseline runs.

The clock drift term (frequency bias), \dot{b} , is estimated in addition to the orbital state vector when using one-way data. For the GRO satellite, the atmospheric drag parameter (ρ_1) can be either estimated or considered. The values in Table 4-7 for ρ_1 and its a priori covariance are for cases in which ρ_1 is estimated.

For the CKF and CEKF estimators, the central body term (GM), and any of the geopotential coefficients can be considered. For one-way data, the clock drift rate (\ddot{b}) can also be considered. The atmospheric drag parameter (ρ_1) can be considered when estimating the GRO orbital state.

V. Evaluation Results

The four estimation algorithms were studied to determine their best performance with data with the baseline error levels. In the case of the EKF, this included tuning the process noise parameters to give optimal results. For the CEKF and the CKF, the selection of the considered parameters and tuning their variances was studied. All baseline runs and their variations used a tracking schedule of 10 minutes every N revolutions of the user satellite and alternating observations of the two TDRSs. Figure 4-2 shows the periods of visibility of TDRS-E and TDRS-W from GRO for 24 hours from the time of epoch (October 1, 1980). The shaded areas represent the data spacing for cases with one contact per revolution. A similar visibility pattern is used for the Landsat-D satellite.

Some representative results taken from the Landsat-D satellite studies are shown in Table 5-1, and some results when the user satellite is GRO are shown in Table 5-2. The run numbers in these tables refer to the run numbers used in references 1, 2, and 3.

The runs are grouped to allow comparison of the performance of an extended estimation (EKF, CEKF) against a batch processor (SBDC, CKF). Statistics for an extended estimator are given for two periods, 9-12 hours and 21-24 hours after the beginning of the data spans. The later period is to assess the estimator accuracy unaffected by transients associated with initializing the estimator. For some of the runs, the differences between the 9-12 hour span and 21-24 hour span evaluations show that the extended estimator has not reached an equilibrium solution at 12 hours, but requires a longer time. In the case of the batch (SBDC, CKF) estimators, the statistics are associated with a

typical ephemeris prediction that uses an initial state derived from processing data spanning the previous 12 hours.

Effect of the Baseline Data Errors

The error in the along-track direction for the Landsat-D B5 EKF run is shown in Figure 5-1. The behavior of these errors is characteristic of the EKF, in which a large initial deviation (reaching, in this case, a maximum of 2549m), is reduced to an acceptable level as the data processing proceeds and the filter achieves an equilibrium solution. For comparison, the along-track error for the L02 SBDC run is shown in Figure 5-2. In this case, Figure 5-2a is a plot of the definitive solution error over the data span, and 5-2b the predictive error after the end of the data. These errors behave in a manner characteristic of a DC estimator, in which the definitive solution errors have a mean of zero. The predictive errors behave as would be expected from the differences in the truth and estimator force models, as shown in Figure 4-1.

The additional errors in the modeling from increased drag on the GRO satellite decrease the accuracy attainable by the estimators, as can be seen by comparing the Table 5-2 baseline results to those in Table 5-1. The statistics for the P12 EKF run as compared to the B5 run show the EKF requiring more than 12 hours to reach an equilibrium solution, and producing a little larger rms and maximum deviation after the equilibrium solution is reached.

The CEKF run 200E, whose along-track errors are plotted in Figure 5-3 is using the J_2 harmonic coefficient as a consider parameter.

Effect of Reduced Data Sets

Using less data, delta-range data only (run H3) or a pass of data every other revolution (runs L5, L12, L14E) does not affect the solution accuracy significantly. When the data is decreased even further, to data only every third revolution, there is some growth in the error, with the run D2 statistics as compared to B5 as an example.

The effect of using less data is more pronounced with the GRO satellite. The CEKF run L13E shows rms and maximum deviations approximately double those in run 200E. This CEKF run is using the Earth geopotential constant (GM) as a consider parameter. Run P24, with along track errors plotted in Figure 5-4, shows that when the EKF estimator has a data pass once every three revolutions, or 6 contacts (360 observations) over 24 hours, approximately 15 hours is required to reach an equilibrium solution for a drag perturbed satellite.

The Effect of TDRS Ephemeris Errors

Runs E4 and L15 are examples of the effect of larger TDRS ephemeris errors in the Landsat-D data. It was found that the estimators perform about as well using only delta-range data as when both range and delta-range data are used as long as the weighting on the range data reflects the larger error in that data type from the TDRSS ephemeris errors. When the TDRS ephemeris errors were not reflected in the range measurement noise (that is, the estimator assumed a more accurate measurement than was available), the estimation accuracy was degraded. Proper use of the range data assumes a good knowledge of the level of error in the TDRS ephemeris, a factor which increases the risk of using that data type.

The SBDC run L15 also included the effect of a TDRS ephemeris update 14 hours after the beginning of the Landsat-D data set.

The first two data spans of the SBDC are data processed with increasing TDRS ephemeris errors, and, as the SBDC processes successive 12 hour spans, the level of the total TDRS ephemeris error becomes less. This can be seen in Figure 5-5 of the along-track errors in the first and fifth data spans. The rms of the predicted solution is 202m for the second span and 139 for the fifth; the maximum deviations are 304m and 190m, respectively. (The statistics given in Table 5-1 are from the first data span).

The effects of additional \dot{L} error in the TDRS ephemeris for the GRO satellite are shown in the runs Q17 of the EKF and G6 of the SBDC in Table 5-2. The SBDC shows an increasing effect as the successive spans of data are processed. The statistics given are from the third data span. At the fifth, they are 323m rms and 507m maximum deviation. The errors in the G1 run, by comparison, stay more uniform over the data arc; the statistics given are for the fifth span of that run.

The SBDC run G15 includes a TDRS ephemeris update at 14 hours. The plot of the along-track error in Figure 5-6 is over the first 12 hours, showing the solution accuracy as the maximum TDRS ephemeris error is approached.

Effect of Onboard Clock Errors

Use of one-way data degrades the solution accuracy as compared to the two-way data results. Landsat-D runs M4, L08 and the GRO run R8, show this. One-way data has increased error due to the user clock errors, especially the frequency bias and drift, and the larger delta-range measurement noise. Also, the estimators must now solve for one or two additional terms with no increase in the amount of data. The EKF requires a larger processing span to achieve an equilibrium solution than when using two-way data, as can be seen in Figure 5-7 of EKF run M4. The SBDC L08 run exhibits the type of errors common to a DC estimator trying to estimate a

quadratic clock error (linear frequency bias error) with a linear equation (constant). The plot of the definitive solution along-track errors, in Figure 5-8, show this effect, with the errors containing a linear term.

Estimating with one-way GRO data is considerably more difficult than with one-way Landsat-D data. Figure 5-9 shows the along-track errors for EKF run R8, estimating the frequency bias for the accurate clock. The effect of the drag errors, and the necessity for solving for the drag parameter, can be seen by comparing Figure 5-9 with the comparable run for Landsat-D, in Figure 5-7.

Replacing the accurate oscillator in the one-way data model with the NASA standard transponder, whose frequency drift is 200 times larger, produces much worse results. The errors in the SBDC grow to hundreds of kilometers when attempting to model this oscillator as one with a constant frequency bias. The EKF run N14 with Landsat-D data, shows that when both the frequency bias and drift are estimated, the solutions are as accurate as with the two-way data. However, this should not be construed as demonstrating that the frequency drift must be estimated for accurate solutions. It is only a demonstration of the need for correctness in the estimator modeling of one-way data as the data is simulated with the same oscillator as is used in the estimator.

The NASA transponder oscillator produces even worse results when used with GRO data. Runs comparable to the EKF run with this data gave solutions accurate only to 1-10 kilometers. All of the estimators need to estimate the frequency drift to perform well with GRO data with the transponder oscillator error.

Effect of Anomalous Data

Data sets were generated in which one or two passes had anomalous data errors; large increases in any or all of the errors sources beyond what is expected by the estimators. If the estimator can recognize that the data pass is in error and edit it, it has virtually no effect on the solution accuracy. If the estimator does not recognize the data pass as having larger errors, then it can, and does, corrupt the solution accuracies. Runs O4 and L17 are two in which the Landsat-D data with anomalous errors were not all edited. Plots of the solution accuracies are shown in Figures 5-10 and 5-11, respectively. For run L17, the bad data occurs at 4^h 45^m after the beginning of the data span. The definitive solution from Figure 5-11a is for the first span in which the data, nearly centered in this span, shows a more significant effect than Figure 5-11b, where the bad data are the first points encountered.

The along-track errors in the two runs with anomalous data in Table 5-2, the T3 EKF run and the G19 SBDC run, are plotted in Figures 5-12 and 5-13, respectively. In both cases the errors are such that the anomalous data are not all edited. The bad data pass for G19 has a significant effect on the second span of the SBDC, as seen in Figure 5-13a, but the estimator is recovering by the fourth span, as shown in Figure 5-13b. The statistics given are those for the second span; for the fourth they are 377m rms and 566m maximum deviation.

VI. Conclusions

These studies have been done by modifying an existing satellite-to-satellite tracking system in an attempt to study relevant data error sources. While it is an analyst's axiom that no simulation can adequately model the real world effects, it does allow some conclusions as to the appropriate procedure for onboard navigation.

- All estimators give solutions using the baseline data sets to an accuracy of 500m or better, often to better than 100m.
- Use of the two-way range data with the delta-range data produces the same results as using the delta-range data alone only as long as the TDRS ephemeris errors are well known and accounted for in the data weighting. If their effect is underestimated, the range data will degrade the solution accuracy.
- The model used for the frequency standard should be examined further to determine appropriate models for estimation of realistic errors. The solution accuracy depends strongly on the accuracy of this estimation when one-way data is used.
- The SBDC estimator needs no tuning for optimal performance with the two-way data.
- The EKF, CEKF, and CKF estimators must be tuned to the specific circumstances for which they are intended for optimal performance. With this data type, these estimators perform best when tuned to respond somewhat slowly to new data.
- The estimator which requires the least processing from the onboard computer is the EKF. The one which requires the most is the CKF.

- The EKF and CEKF need between 6-15 hours to reach an equilibrium solution, depending on the data type and frequency. The SBDC and CKF need 2 to 4 iterations to converge to an acceptable solution.

REFERENCES

1. CSC/TM-80/6176, Onboard Orbit Determination with Tracking and Data Relay Satellite System (TDRSS) Data, Volume 1, Extended Kalman Filter (EKF) Evaluation, A. C. Long, P. S. Gural, October 1980
2. CSC/TM-80/6234, Onboard Orbit Determination with TDRSS Data, Volume 2, Sliding Barch Differential Corrector (SBDC) Evaluation, K. A. Preiss, J. B. Dunham, in preparation
3. CSC/TM-80/6235, Onboard Orbit Determination with TDRSS Data, Volume 3, The Consider Filter Evaluation, J. B. Dunham and H. M. Sielski, in preparation
4. CSC, Goddard Trajectory Determination System Research and Development (GTDS R&D) User's Guide (draft), August 1978
5. CSC/SD-79/6032, The Research and Development Goddard Trajectory Determination System (R&D GTDS) Filter Program Software Specifications and User's Guide, J. B. Dunham, December 1968
6. Mathematical Theory of the Goddard Trajectory Determination System, J. O. Cappellari, C. E. Velez, and A. J. Fuchs (eds), GSFC, X-582-76-77, April 1979
7. NASA, End-to-End Data System (NEEDS) Ancillary Data and Support Computing (ADSC) Concept Document, NEEDS/ADSC Team, June 1980

Table 4-1. Landsat-D and GRO Orbital Elements, Area, and Mass

PARAMETER	LANDSAT-D	GRO
EPOCH	OCTOBER 1, 1980	OCTOBER 1, 1980
COORDINATE SYSTEM	TRUE OF DATE	TRUE OF DATE
SEMIMAJOR AXIS (km)	7086.901	6778.140
ECCENTRICITY	0.001	0.0017
INCLINATION (deg)	98.181	28.0
LONGITUDE OF ASCENDING NODE (deg)	354.878	0.0
ARGUMENT OF PERIGEE (deg)	180.0	0.0
MEAN ANOMALY (deg)	0.0	0.0
PERIOD (min)	98.956	92.56
AREA (m ²)	20.0	20.0
MASS (kg)	1700.0	1700.0

7657/80

Table 4-2. Data Simulation Measurement Errors

PARAMETER	BASELINE STANDARD DEVIATION	
	ONE-WAY DATA	TWO-WAY DATA
Random Range Error (m)	-	1
Random Delta-Range Error (cm)	10	1
Range Measurement Bias (m)	-	7
Delta-Range Measurement Bias (cm)	+	-

⁺The delta-range measurement bias due to the user clock is
 = 60,000 + 0.0069t cm for the accurate clock,
 = 300,000 + 0.69t cm for the NASA standard transponder,
 t measured in seconds from the clock epoch.

Table 4-3. Data Simulation TDRS Ephemeris Error Model

PARAMETER	VALUE
PERIOD OF SINUSOID ¹ (hr)	24
RADIAL AMPLITUDE (m)	35
CROSS-TRACK AMPLITUDE (m)	35
ALONG-TRACK AMPLITUDE (m)	80
ALONG-TRACK GROWTH RATE (m/day)	250

7526/80

¹SINUSOIDAL PERIOD FOR RADIAL, CROSS-TRACK, AND ALONG-TRACK TDRS EPHEMERIS ERRORS.

Table 4-4. Data Simulation Quadratic User-Clock Error Model

COEFFICIENT	ONE-WAY DATA		TWO-WAY DATA
	NASA STANDARD TRANSPONDER	ACCURATE ONBOARD CLOCK	PERFECT CLOCK
USER-CLOCK BIAS (sec)	0	0	0
USER-CLOCK DRIFT (sec/sec)	1×10^{-6}	2×10^{-7}	0
USER-CLOCK DRIFT RATE (sec/sec/day)	2×10^{-7}	2×10^{-9}	0

7526/80

Table 4-5. Dynamic Models

PARAMETER	DATA SIMULATION VALUE	EKF/CEKF VALUE	SBDC/CKF VALUE
GEOPOTENTIAL	15x15, GEM-9	8x8, GEM-1	8x8, GEM-7
RESONANCE (GRO ONLY)	YES	NO	NO
SOLAR FLUX	150×10^{-22} watt/m ² /Hz	200×10^{-22} watt/m ² /Hz	200×10^{-22} watt/m ² /Hz
AERODYNAMIC DRAG COEFFICIENT	2.0	2.2	2.2
SUN AND MOON	YES	YES	NO
SOLAR RADIATION PRESSURE	NO	NO	NO
INTEGRATOR	COWELL 12th-ORDER	RUNGE-KUTTA 3 (4+)	RUNGE-KUTTA 3 (4+) (CKF) COWELL 12th-ORDER (SBDC)

Table 4-6. Error Growth in Ephemeris over 12 Hours

SATELLITE	MAX. POS. DIFFERENCE (M)			
	ΔH	ΔC	ΔL	ΔR
LANDSAT-D	45.	94.	1232.	1235.
GRO	367.	103.	26573.	26575.

Table 4-7. Estimator Solve-for and Consider Parameters

PARAMETERS	ONE-WAY DATA	TWO-WAY DATA
$x, y, z, \dot{x}, \dot{y}, \dot{z}$	solve	solve
b	solve	-
\dots		
b		
EKF and SBDC	ignore/solve	-
CKF and CEKF	ignore/solve/ consider	-
ρ_1 (GRO only)		
EKF and SBDC	solve	solve
CKF and CEKF	solve/ consider	solve/ consider
GM CKF and CEKF	consider	consider
geopotential harmonic coefficients		
CKF and CEKF	consider	consider

Table 4-8. A Priori Values and Measurement Standard Deviations

PARAMETER	BASELINE INPUT VALUE	
	ONE-WAY DATA	TWO-WAY DATA
A PRIORI STATE OFFSETS		
X, Y, Z	100 m	100 m
$\dot{X}, \dot{Y}, \dot{Z}$	30 cm/sec	30 cm/sec
A PRIORI USER CLOCK PARAMETERS		
b (BIAS)	0 sec	-
\dot{b} (DRIFT)		
NASA STANDARD TRANSPONDER	1.1×10^{-6} sec/sec	-
ACCURATE ONBOARD CLOCK	2.2×10^{-7} sec/sec	-
\ddot{b} (DRIFT RATE)	0 sec/sec/day	-
A PRIORI ρ_1	0.0	0.0
A PRIORI COVARIANCES (EKF, CKF, & CEKF)		
X, Y, Z	0.1 km ²	0.1 km ²
$\dot{X}, \dot{Y}, \dot{Z}$	1.0 m ² /sec ²	1.0 m ² /sec ²
\dot{b}	1×10^{-6} sec/sec	-
ρ_1 (GRO ONLY)	1.0	1.0
A PRIORI COVARIANCES (SBDC)		
X, Y, Z	∞	∞
$\dot{X}, \dot{Y}, \dot{Z}$	∞	∞
\dot{b}	∞	-
ρ_1 (GRO ONLY)	∞	∞
STANDARD DEVIATION OF MEASUREMENT ERROR		
RANGE	-	40 m
DELTA-RANGE	10 cm	1 cm

LANDSAT-D

Run	Estimator	Data Type	Tracking Schedule	rms/max position deviations (m)			Data Error Model
				9 ^h - 12 ^h	typical 3hr prediction	21 ^h - 24 ^h	
B5 L02	EKF SBDC	2-Way $\rho, \Delta\rho$	1 Rev	78/130 -	81/124	41/65 -	baseline
H3	EKF	2-Way $\Delta\rho$	1 Rev	66/95	-	49/82	baseline
C5 L12 L14E	EKF SBDC CEKF	2-Way $\rho, \Delta\rho$	2 Rev	67/99 - 61/92	- 120/174 -	39/55 - 88/134	baseline
D2	EKF	2-Way $\rho, \Delta\rho$	3 Rev	83/162	-	73/119	baseline
E4	EKF	2-Way $\rho, \Delta\rho$	1 Rev	41/85	-	-	8H, 8C
L15	SBDC	2-Way $\Delta\rho$	1 Rev	-	187/262	-	8H, 8C, TDRS Ephemeris Update
M4 L08	EKF SBDC	1-Way $\Delta\rho$	1 Rev	282/418 -	- 345/531	87/169 -	accurate clock
N14	EKF	1-Way $\Delta\rho$	1 Rev	110/190	-	47/92	NASA transponder, b estimated
O4	EKF	2-Way $\rho, \Delta\rho$	1 Rev	66/95	-	140/228	anomalous data 13hrs ρ error = 7 km $\Delta\rho$ error = 300 cm
L17	SBDC	2-Way $\rho, \Delta\rho$	1 Rev	-	58/101	-	anomalous data 5hrs ρ error = 5 km $\Delta\rho$ error = 500cm

Table 5-1. Results for Landsat-D

Run	Estimator	Data Type	Tracking Schedule	rms/max position deviations (m)			Data Error Model
				9h - 12h	typical 3hr prediction	21h - 24h	
P12 200E	EKF CEKF	2-Way $\rho, \Delta\rho$	1 Rev	141/234 174/274	- -	60/88 64/139	baseline
G1	SBDC	2-Way $\Delta\rho$	1 Rev	-	252/420	-	baseline
113E	CEKF	2-Way $\rho, \Delta\rho$	2 Rev	368/637	-	120/230	baseline
P24	EKF	2-Way $\rho, \Delta\rho$	3 Rev	1090/2048	-	102/157	baseline
Q17 G6	EKF SBDC	2-Way $\Delta\rho$	1 Rev	173/315 -	- 245/380	109/194 -	4L
G15	SBDC	2-Way $\Delta\rho$	1 Rev	-	174/249	-	8H, 8C, TDPS Ephemeris Update
R8	EKF	1-Way $\Delta\rho$	1 Rev	306/453	-	129/235	Accurate clock
T3 G19	EKF SBDC	2-Way $\Delta\rho$	1 Rev	162/248 -	- 693/896	226/379 -	anomalous data 13hrs $\Delta\rho$ error = 300 cm

Table 5-2. Results for GRO

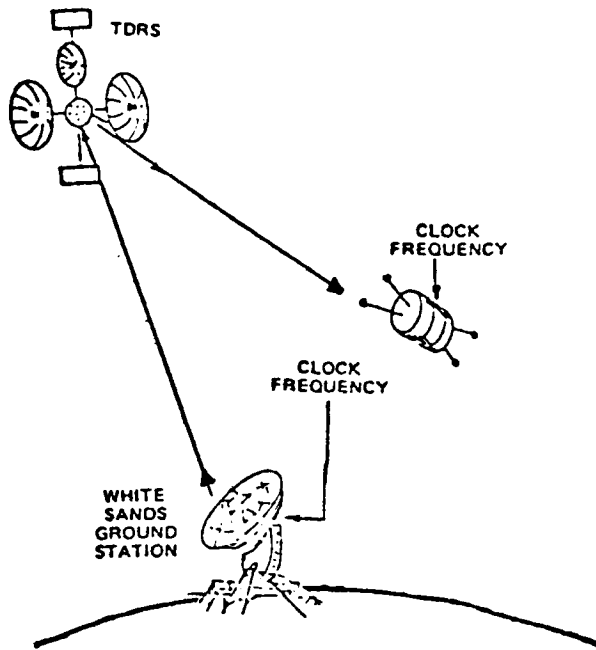


Figure 2-1. One-Way Tracking Signal Geometry

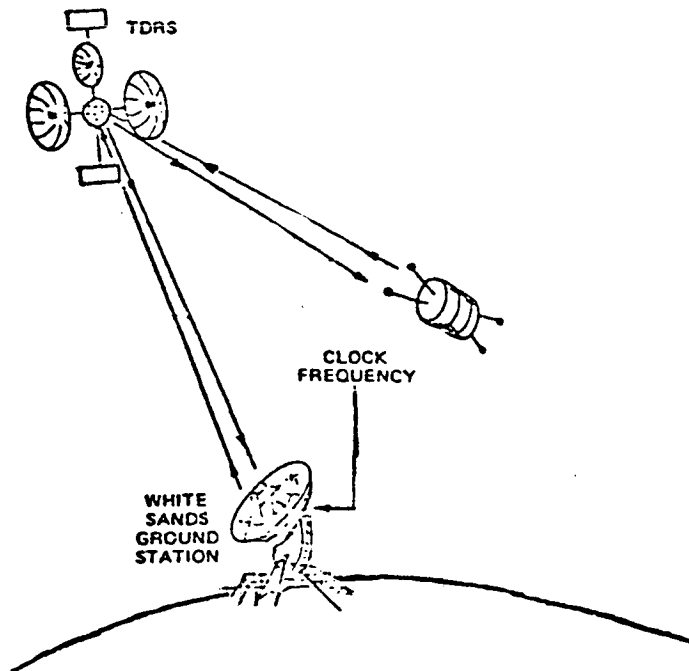


Figure 2-2. Two-way Tracking Signal Geometry

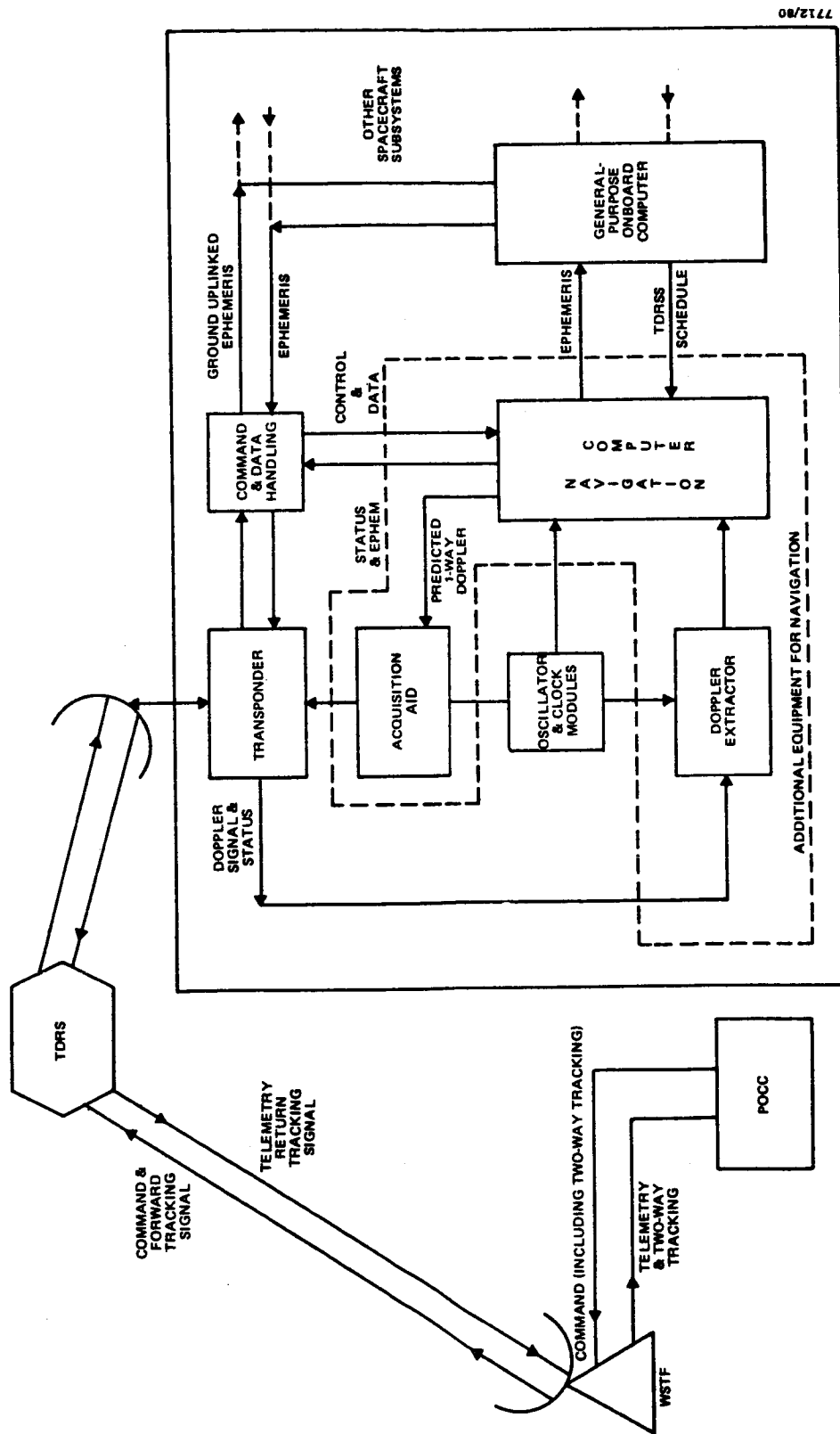


Figure 2-3. One-Way and Two-Way Tracking With TDRSS

EKF

- state update at each observation
- simple process noise covariance model
$$Q = \dot{Q} (t_i - t_{i-1})$$
- tunable parameters
 - a priori covariance
 - \dot{Q} matrix

SBDC

- State update at epoch
- Data in 12-hour spans, new solution generated when each pass of data is collected
- Initial state solution from previous data span propagated to new epoch
- No a priori covariance

CKF, CEKF

- State update at epoch (CKF) or each observation (CEKF)
- Consider covariance used instead of process noise
- Tunable parameters
 - a priori covariance
 - consider parameter selection and variance

Figure 3-1. Estimator Characteristics

given the initial state, $X_{k-1} = \hat{X}_{k-1}$, the covariance, P_{k-1} , and an observation Y_k

1. Propagate to t_k to obtain X_k
state: $\dot{X}_k = F(X, t_k)$ with X_{k-1} as the initial conditions
state transition matrix:

$$\dot{\Phi}(t, t_{k-1}) = A(t) \Phi(t, t_{k-1}) \text{ with } \Phi(t_{k-1}, t_{k-1}) = I$$

the initial conditions,

$$\text{and where } A(t) = \left| \frac{\partial F}{\partial X} \right| \text{ evaluated at } X = X_{k-1}$$

2. Propagate the covariance to t_k

$$\bar{P}_k = \Phi(t_k, t_{k-1}) P_{k-1} \Phi^T(t_k, t_{k-1}) + \dot{Q} \star (t_k - t_{k-1})$$

where \dot{Q} is the state process noise covariance rate.

3. Compute observation (G_k), residual (y_k), and observation partial derivatives (H_k^k)

$$G_k = G(X_k, t_k)$$

$$y_k = Y_k - G_k$$

$$H_k = \left| \frac{\partial G}{\partial X} \right| \text{ evaluated at } X = X_k$$

4. Compute gain (K_k), update covariance (P_k), and state (\hat{X}_k)

$$K_k = \bar{P}_k H_k^T [H_k \bar{P}_k H_k^T + R_k]^{-1} \text{ where } R_k \text{ is the observation weight}$$

$$P_k = [I - K_k H_k] \bar{P}_k$$

$$\hat{X}_k = X_k + K_k y_k$$

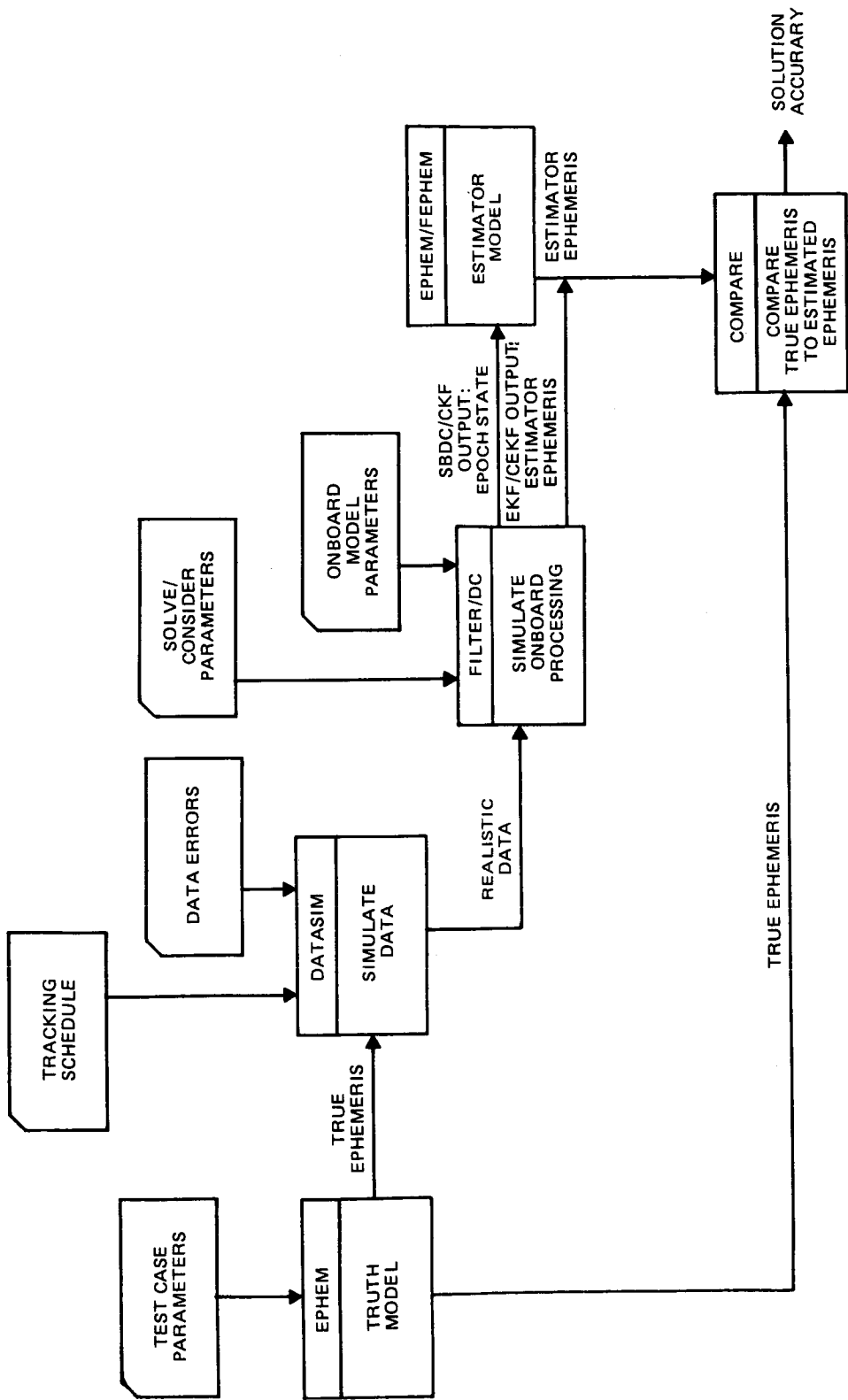
5. If there is more data, return to step 1.

Figure 3-2. EKF Operational Flow

Input: state $X(t_0)$

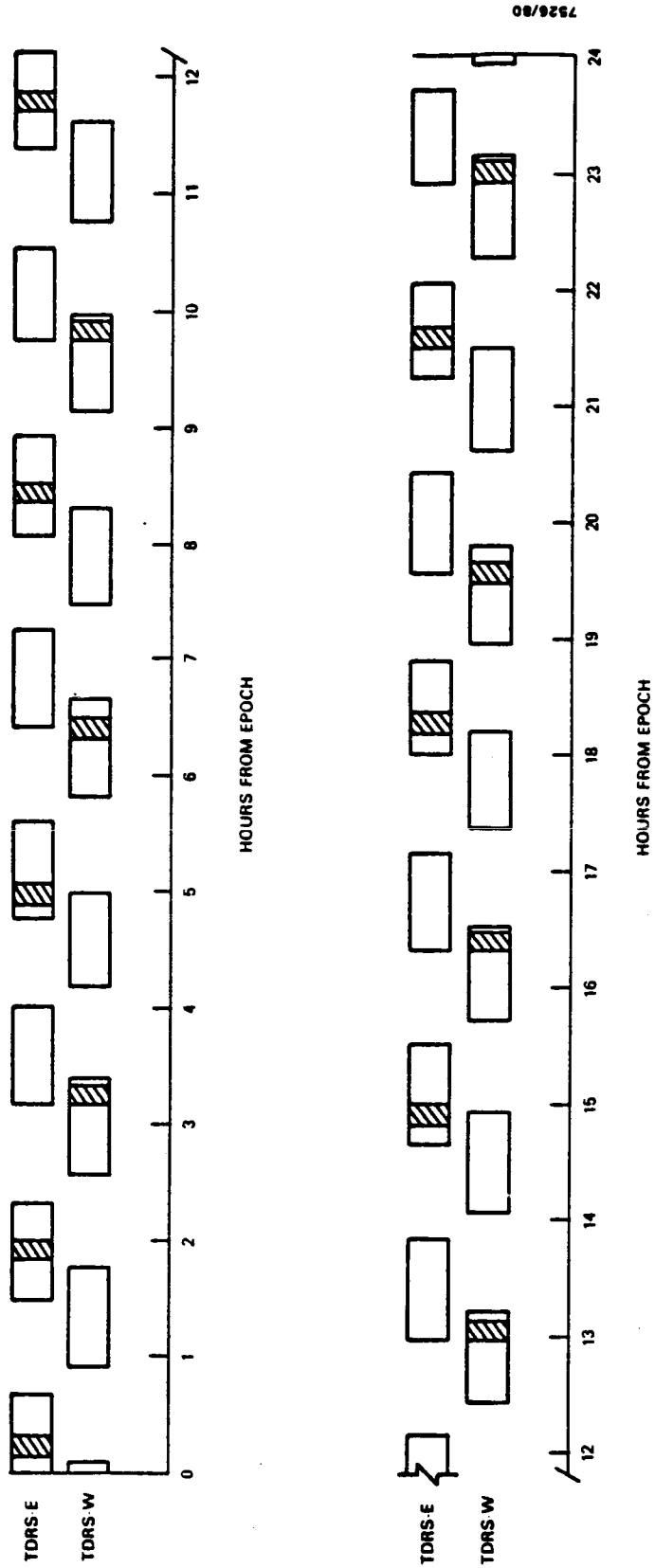
1. Select observation span, Y_k to Y_ℓ , and new epoch, t_k . Propagate state to the new epoch, t_k .
2. Integrate state and state transition matrix to each observation
state: $\dot{X} = F(X,t)$ with $X(t_i)$ as the initial conditions
state transition: $\dot{\Phi}(t,t_i) = A(t)\Phi(t,t_i)$
with $\Phi(t_i,t_i) = I$ as the initial conditions
3. Compute observation, residual, and observation partials
 $G_i = G(X_i, t_k)$
 $y_i = Y_i - G_i$
 $H_i = \tilde{H}_i \Phi(t_i, t_k)$, where \tilde{H}_i is the observation partials at t_i
4. When all observations are processed, compute update at epoch, t_k ,
 $\hat{x}_k = (H^T R H)^{-1} H^T R y$, where R is the observation weighting matrix
 $\hat{X}_k = X_k + \hat{x}_k$
5. Determine if the SBDC has converged over this span. If not, repeat steps 2 to 4.
If it has, go to step 1 and select the next data span.

Figure 3-3. SBDC Flow



7712/80

Figure 4-1. Evaluation Procedure for TDRSS Study



- NOTES: 1. EPOCH - OCTOBER 1, 1980.
 2. SHADED AREAS CORRESPOND TO ONE PASS PER REVOLUTION DATA SET.

Figure 4-2. Contacts for the Every Revolution Case for GRO

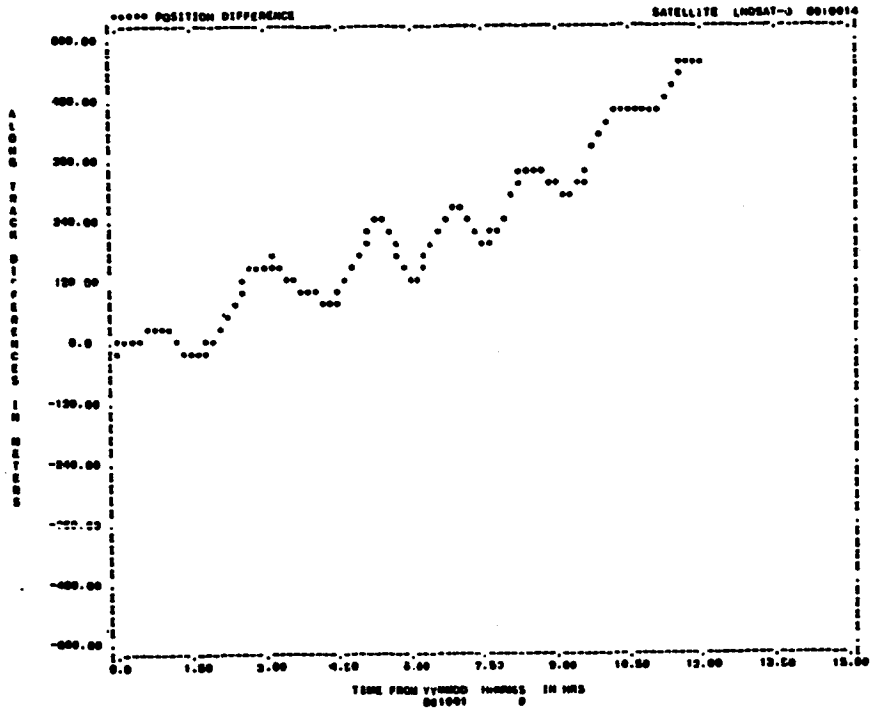


Figure 4-3. Along-Track Error Growth Over 12 Hours for Landsat-D

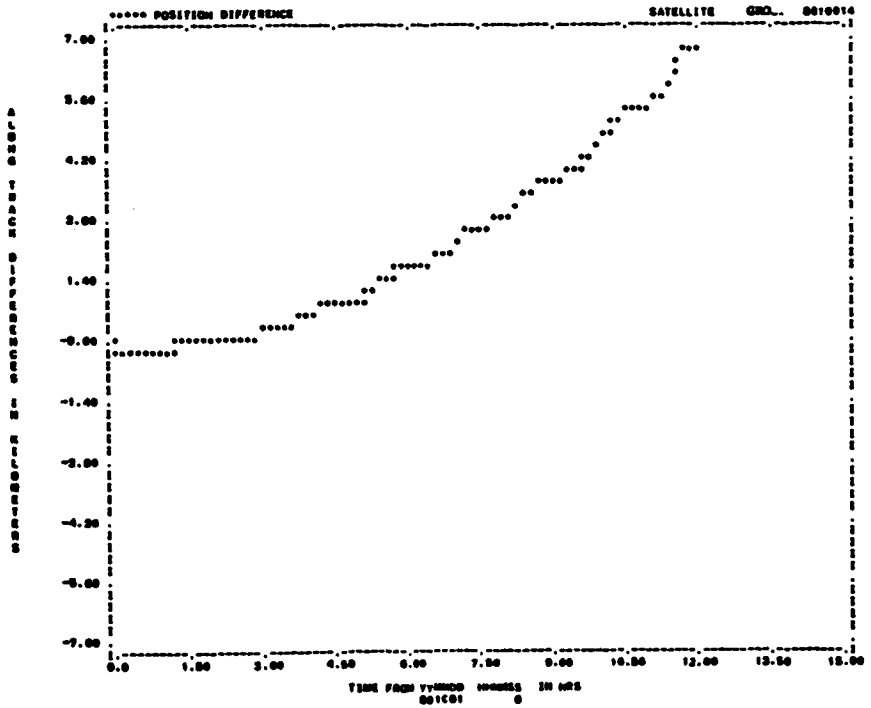
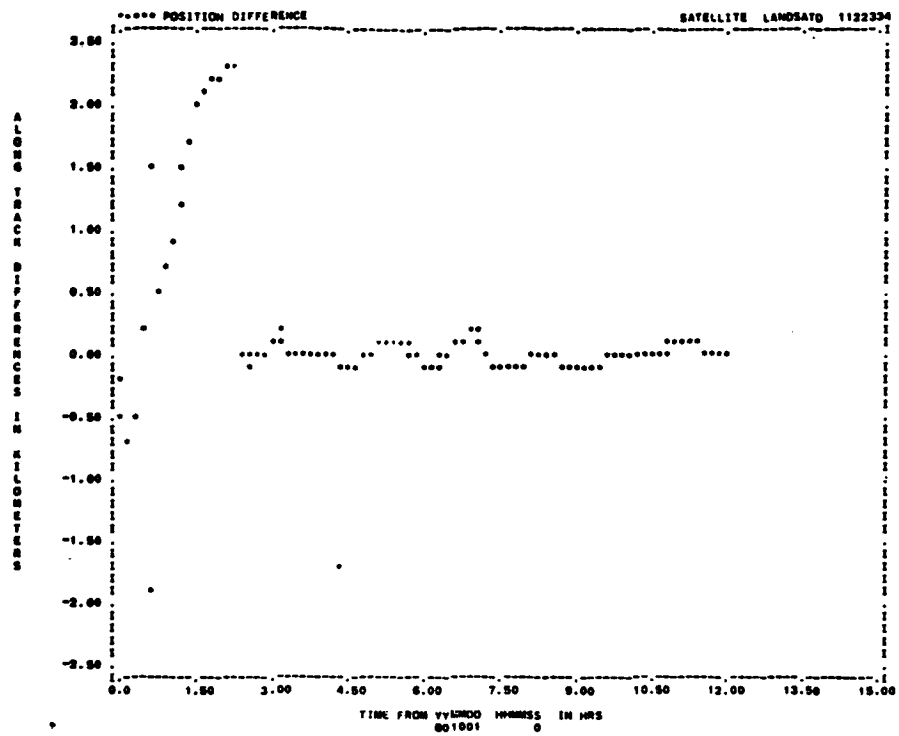
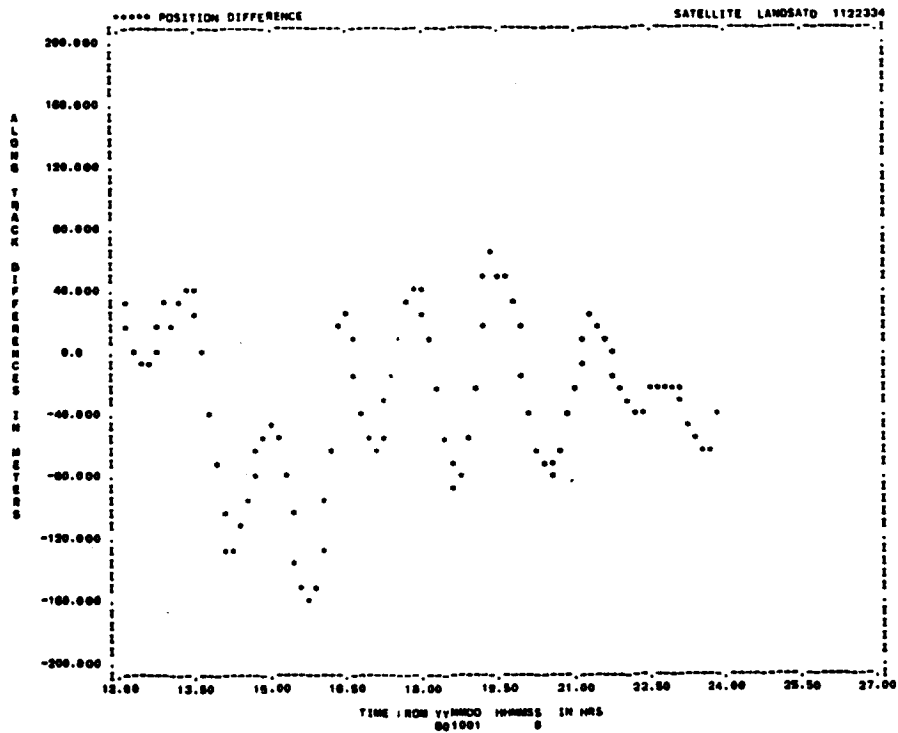


Figure 4-4. Along-Track Error Growth Over 12 Hours for GRO

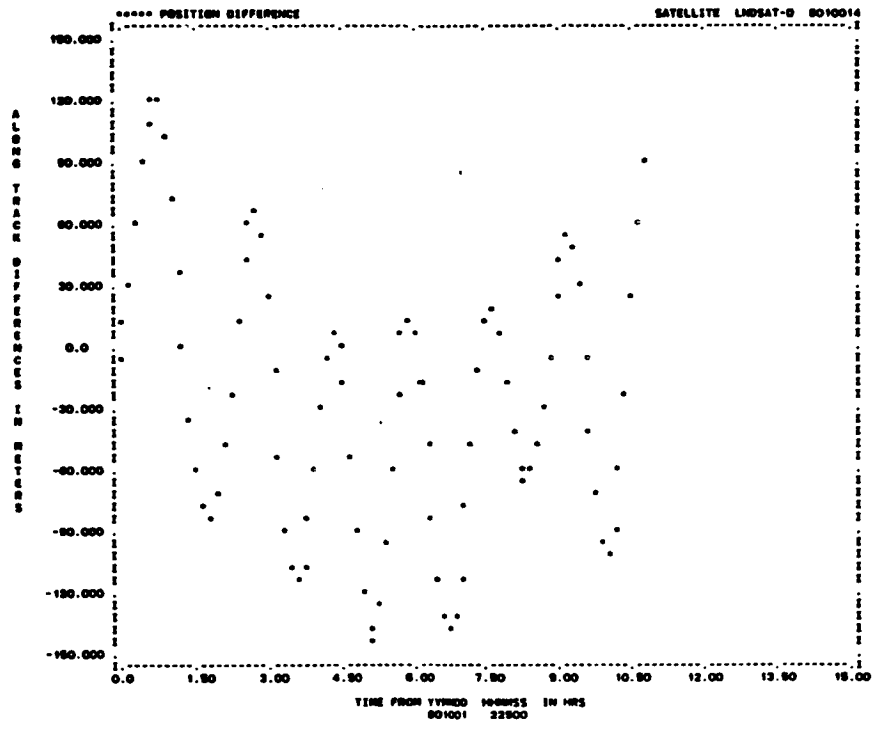


a. 0 to 12 hours

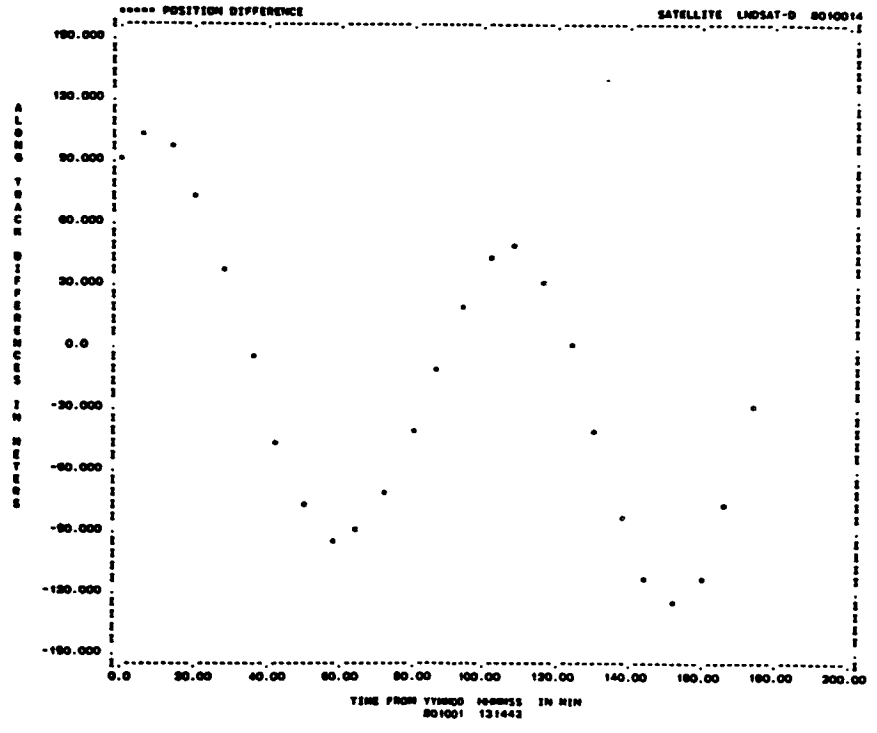


b. 12 to 24 hours

Figure 5-1. Along-Track Error for EKF Run B5

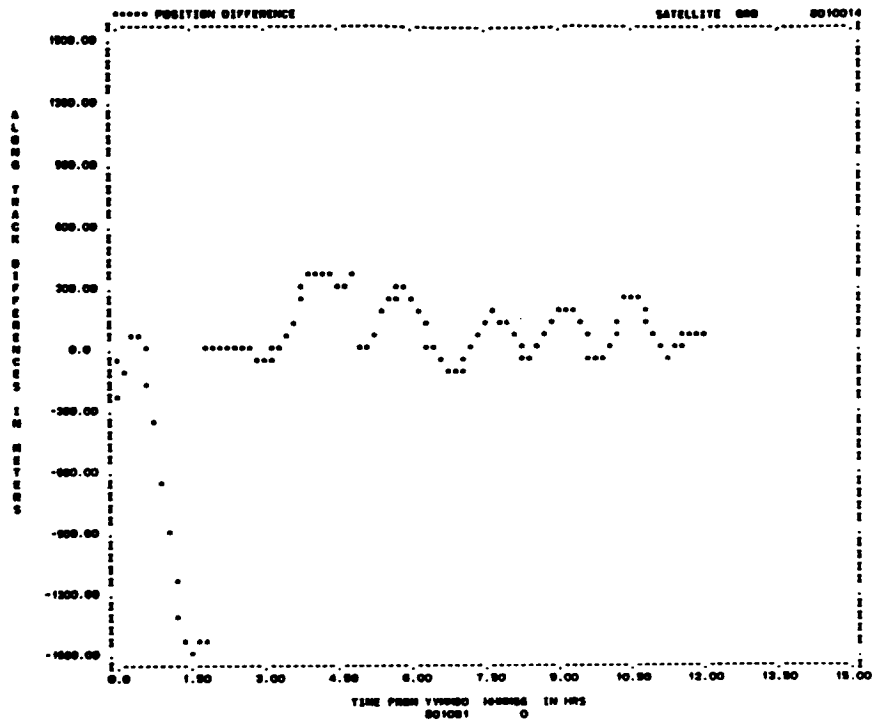


a. Definitive Arc

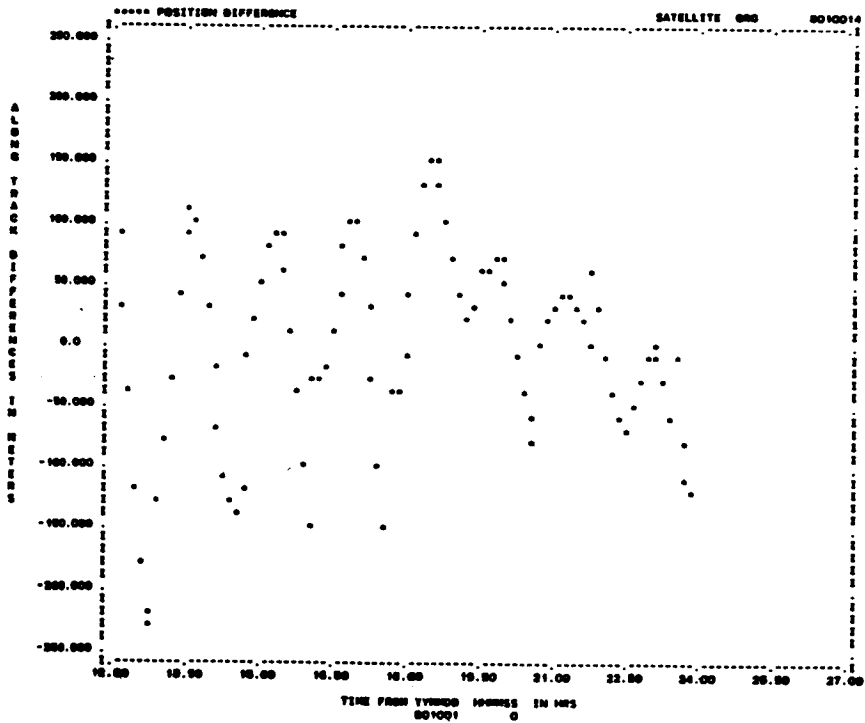


b. Predictive Arc

Figure 5-2. Along-Track Error for SBDC Run LO2

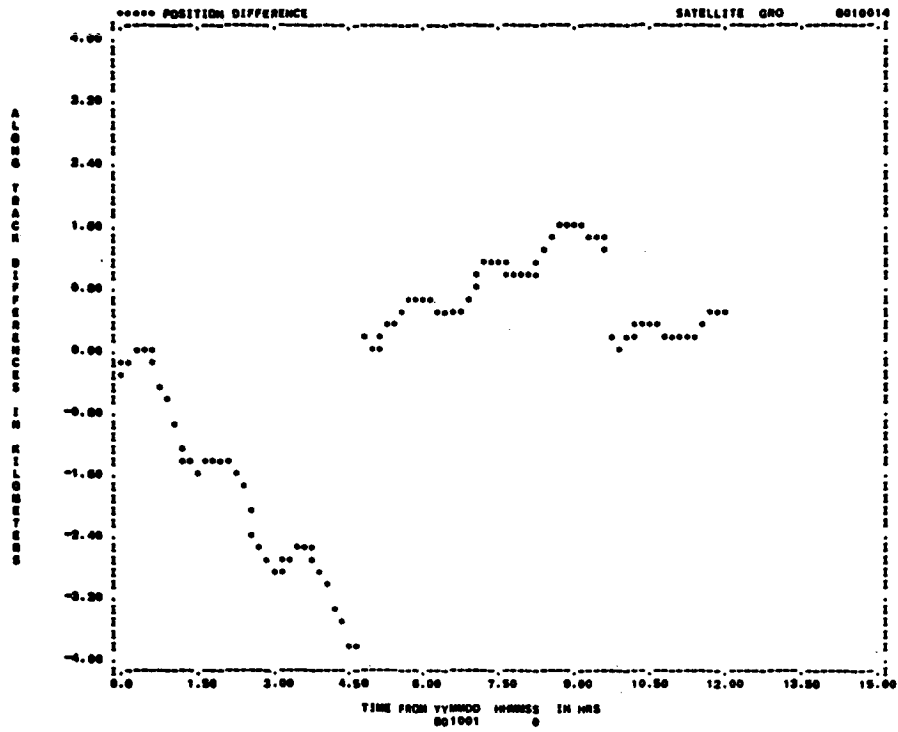


a. 0 to 12 Hours

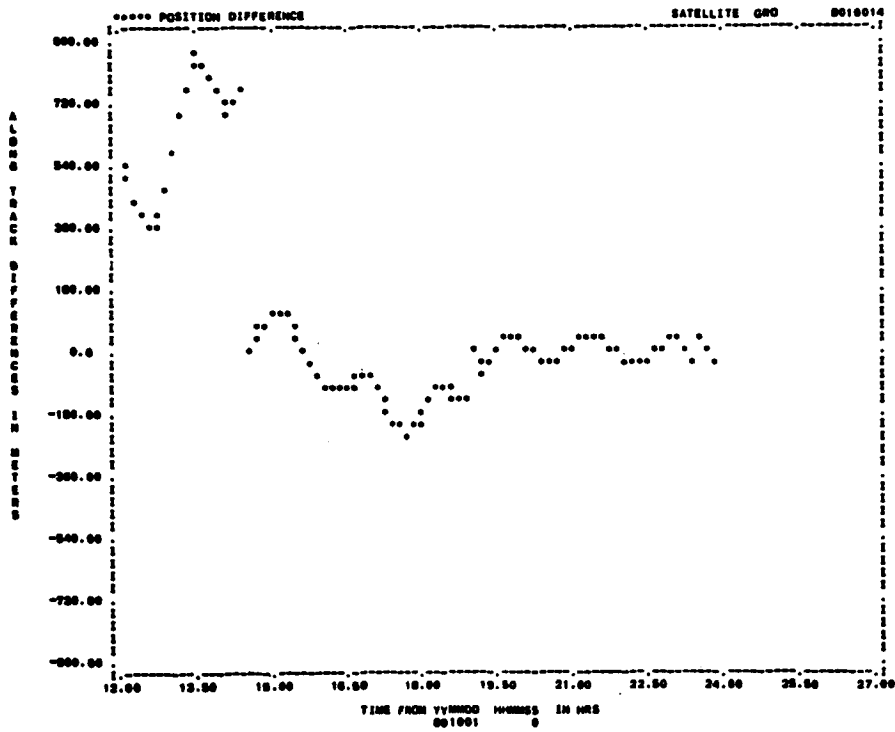


b. 12 to 24 Hours

Figure 5-3. Along-Track Error for CEKF Run 200E

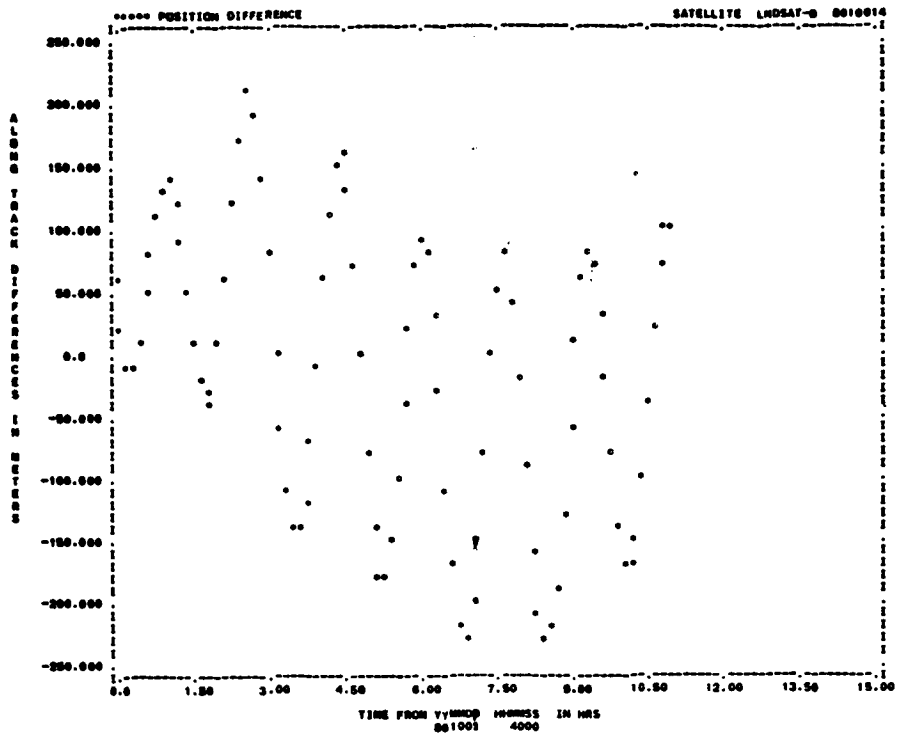


a. 0 to 12 Hours

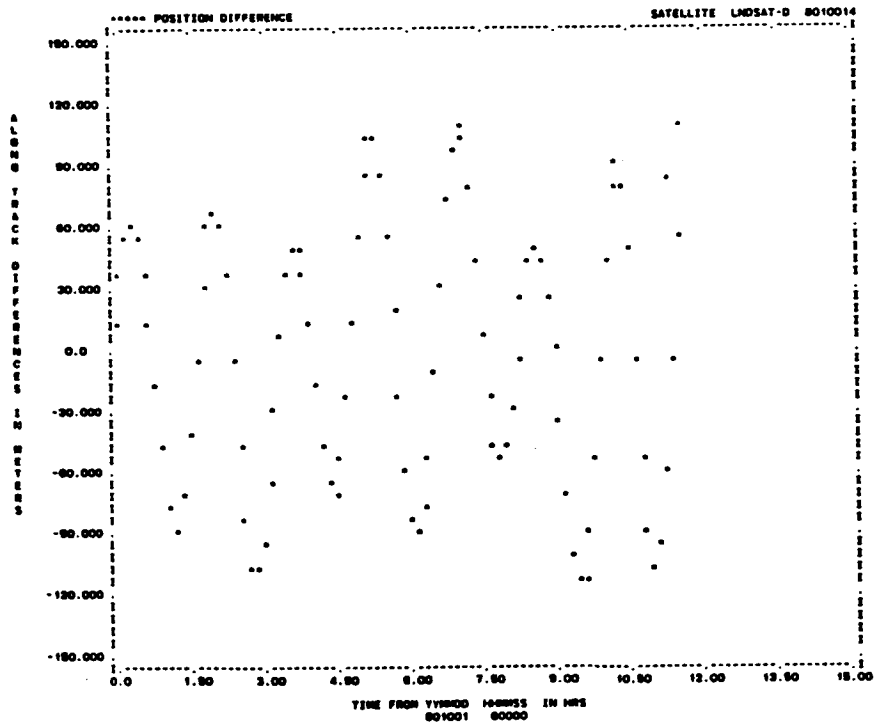


b. 12 to 24 Hours

Figure 5-4. Along-Track Error for EKF Run P24



a. First Span



b. Fifth Span

Figure 5-5. Along-Track Error for SBDC Run L15

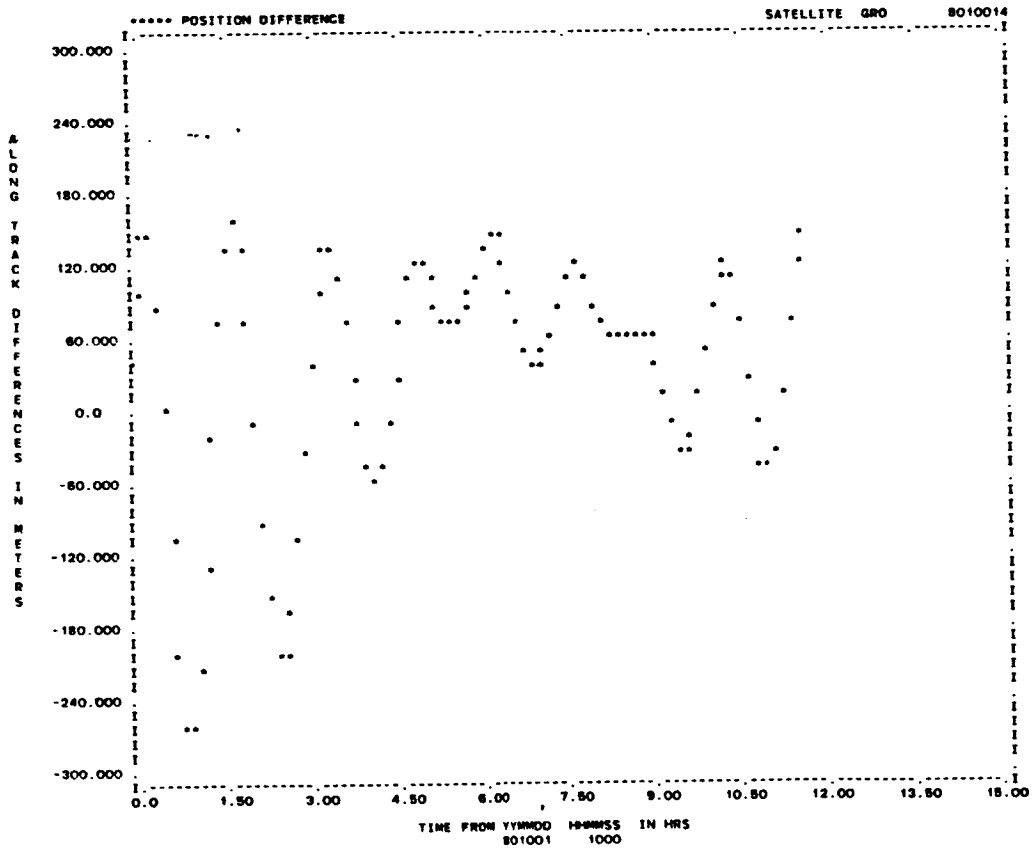
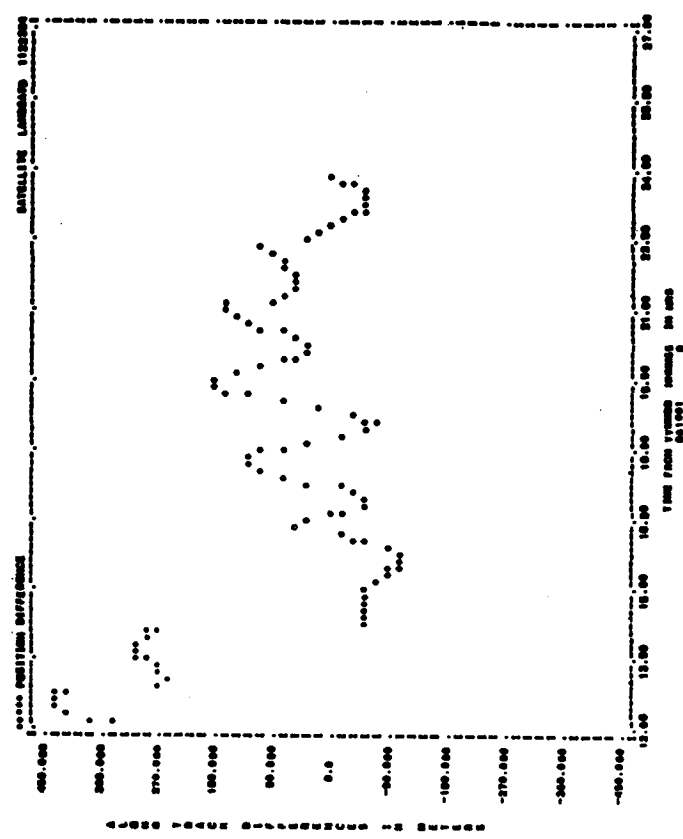
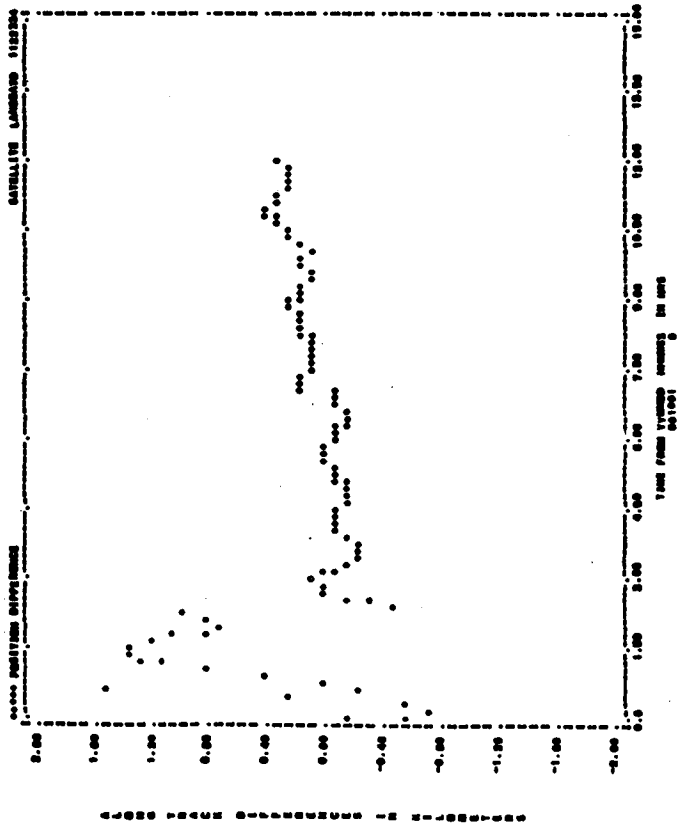


Figure 5-6. Along-Track Error for SBDC Run G15



b. 12 to 24 Hours



a. 0 to 12 Hours

Figure 5-7. Along-Track Errors for EKF Run M4

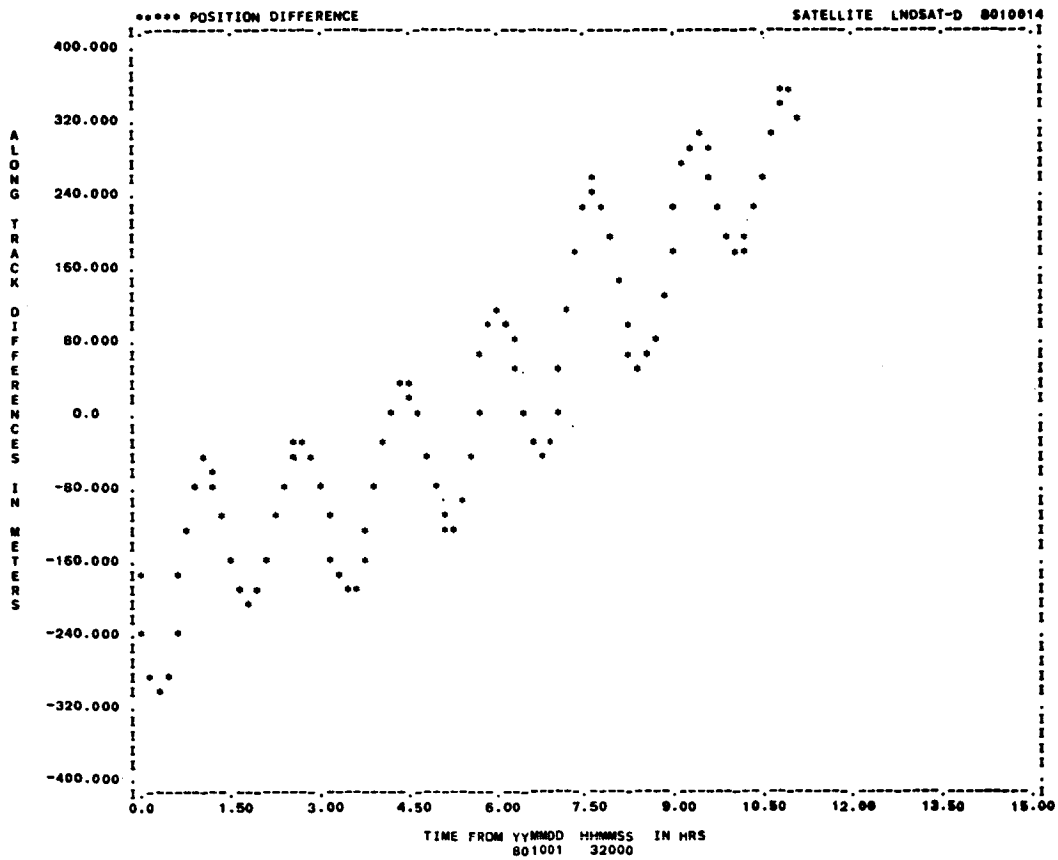
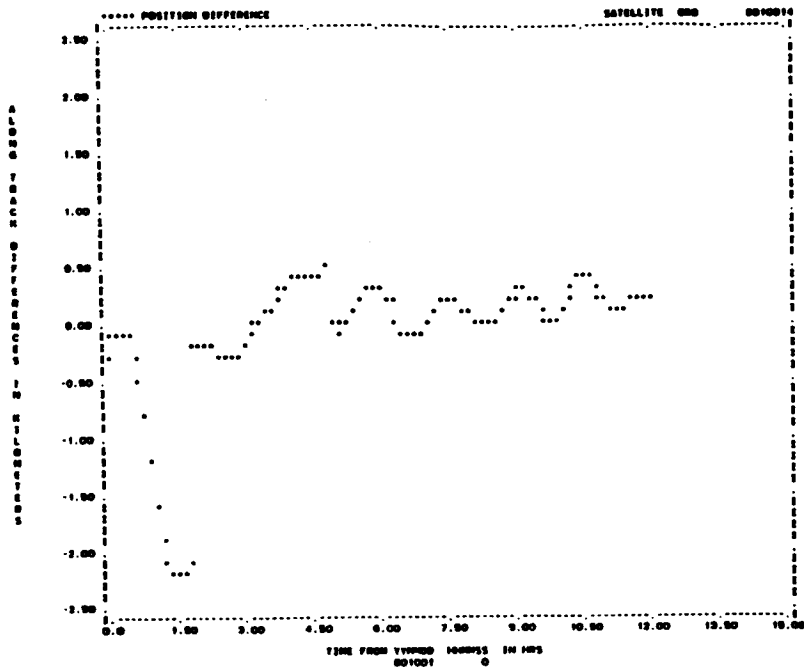
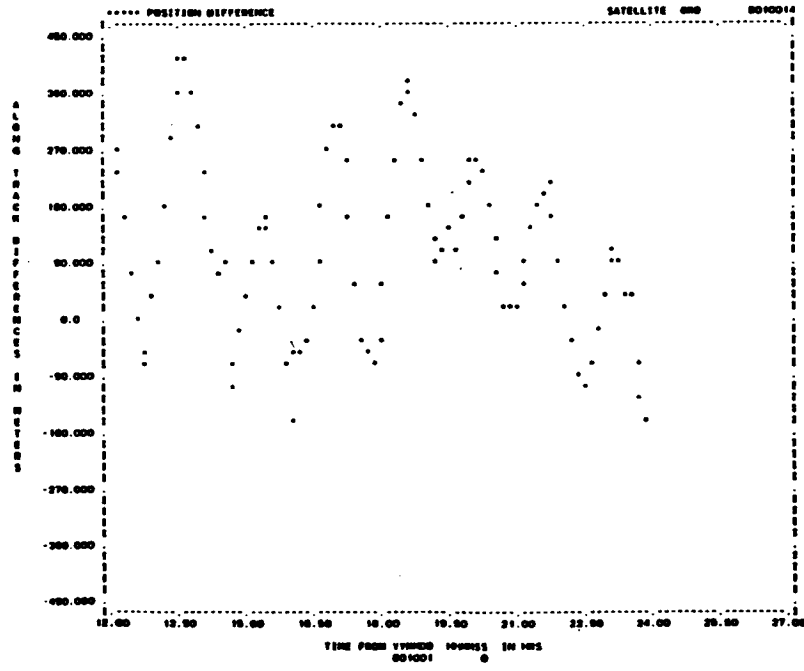


Figure 5-8. Along-Track Error for SBDC Run LO8

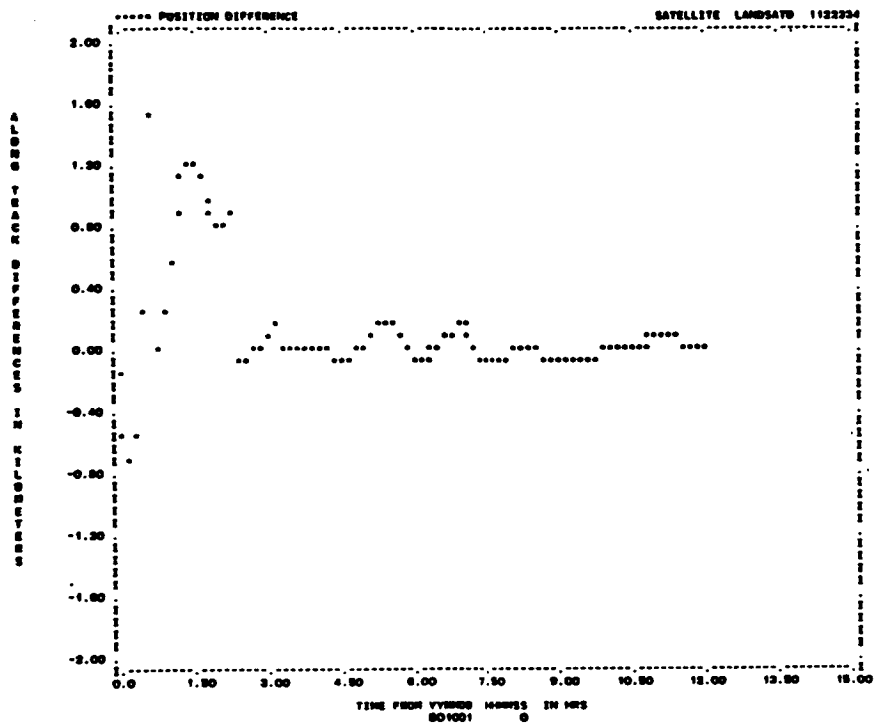


a. 0 to 12 Hours

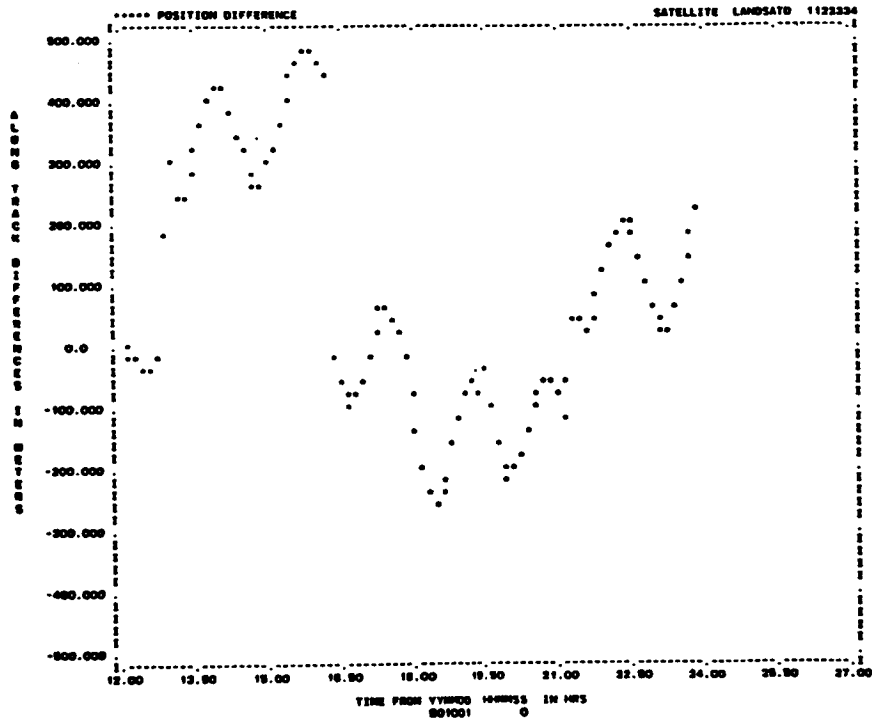


b. 12 to 24 Hours

Figure 5-9. Along-Track Error for EKF Run R8

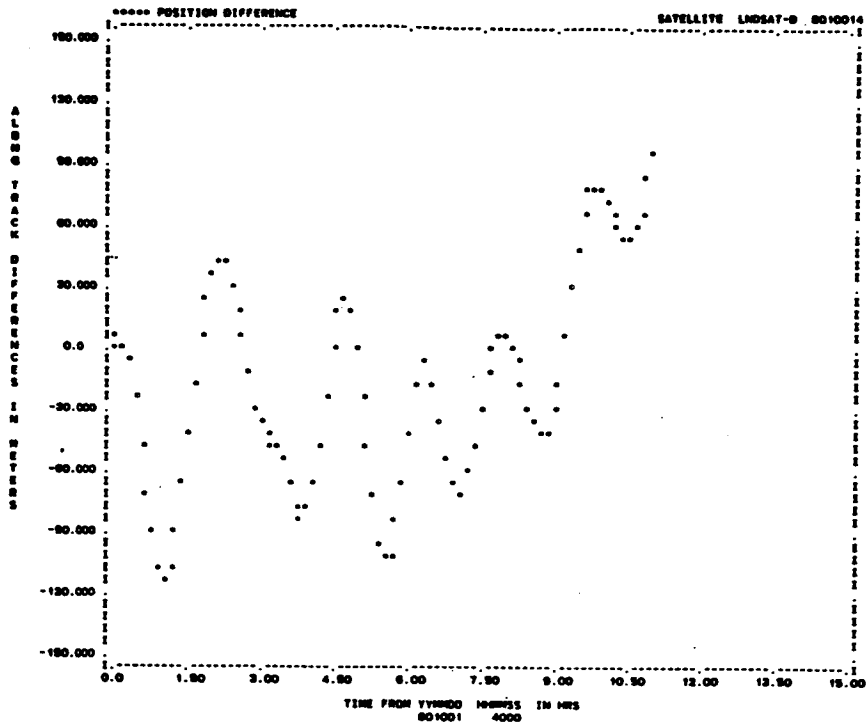


a. 0 to 12 Hours

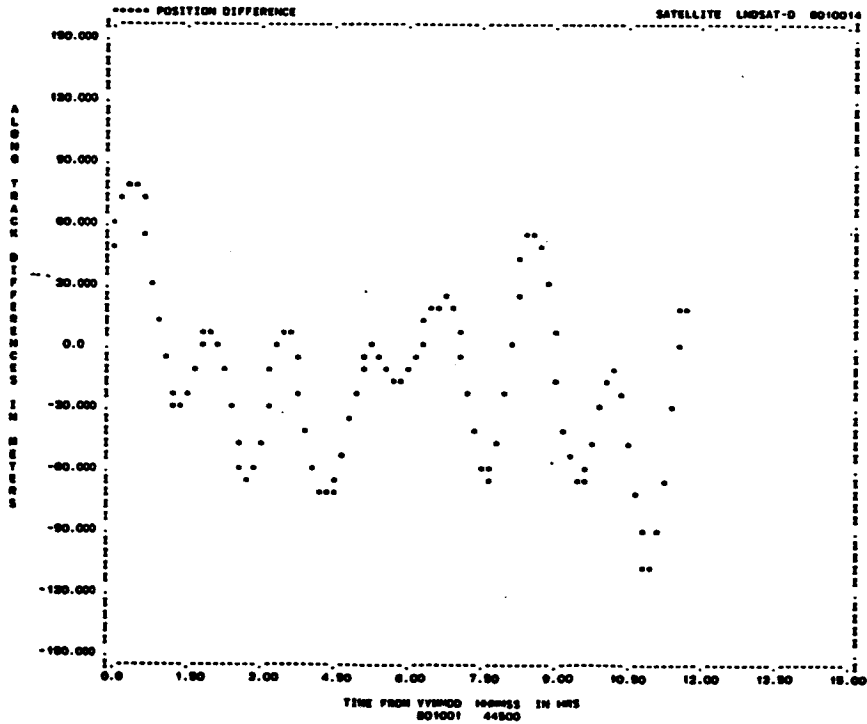


b. 12 to 24 Hours

Figure 5-10. Along-Track Error for EKF Run 04

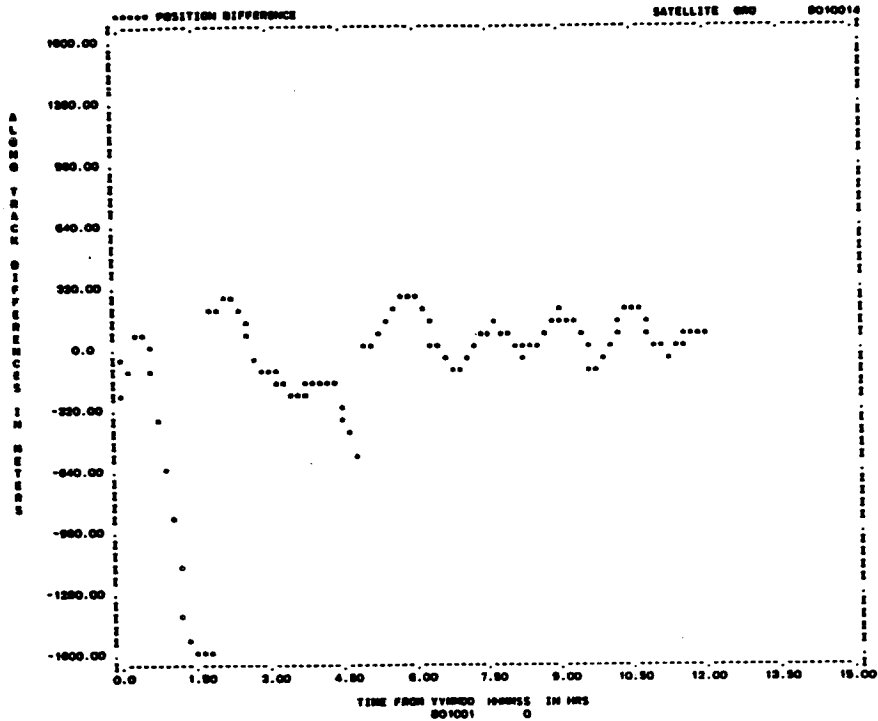


a. First Span

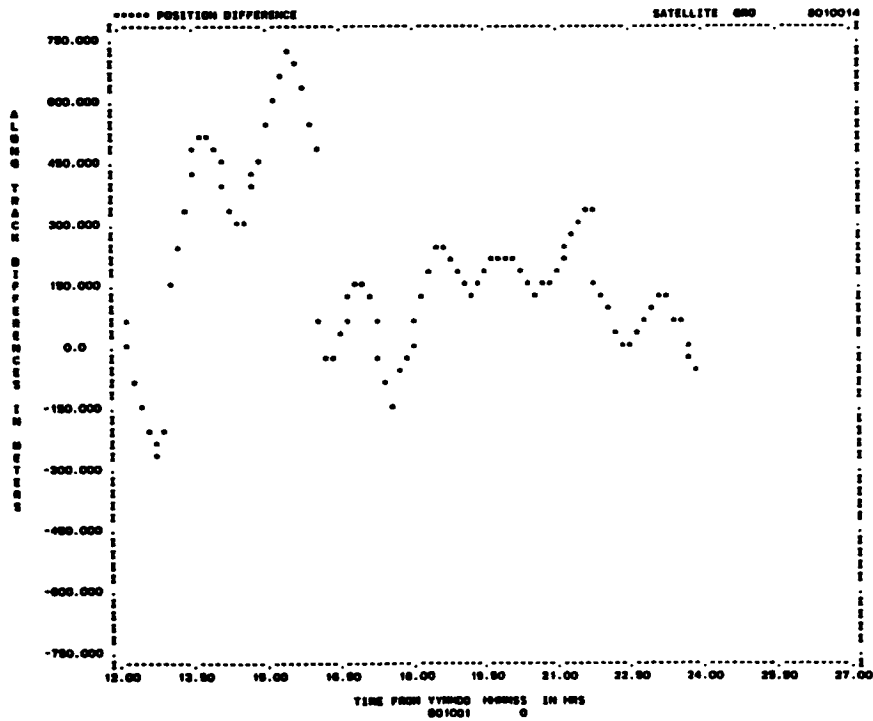


b. Fourth Span

Figure 5-11. Along-Track Errors for SBDC Run L-17

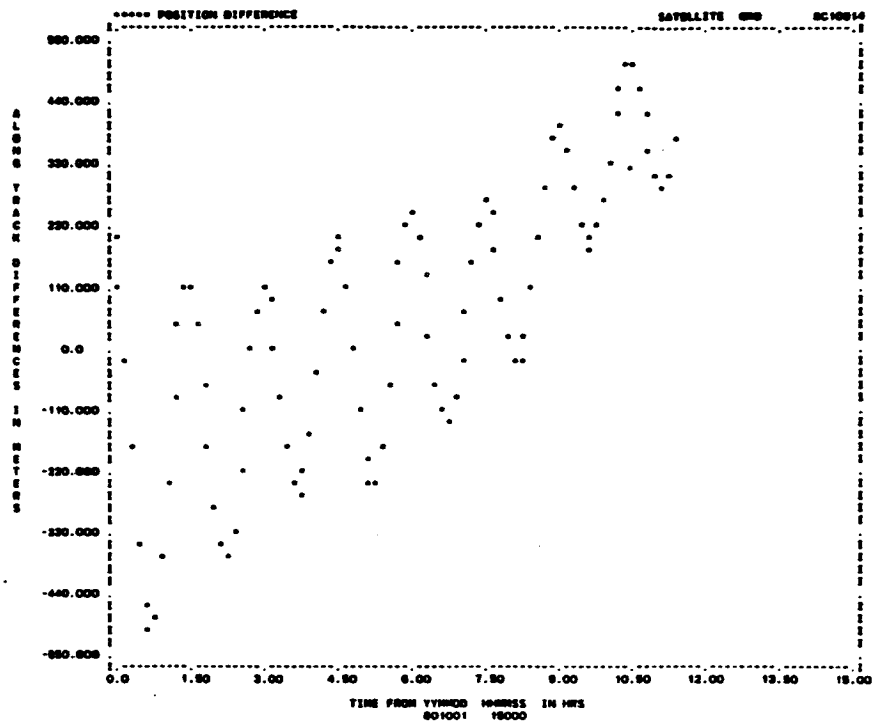


a. 0 to 12 Hours

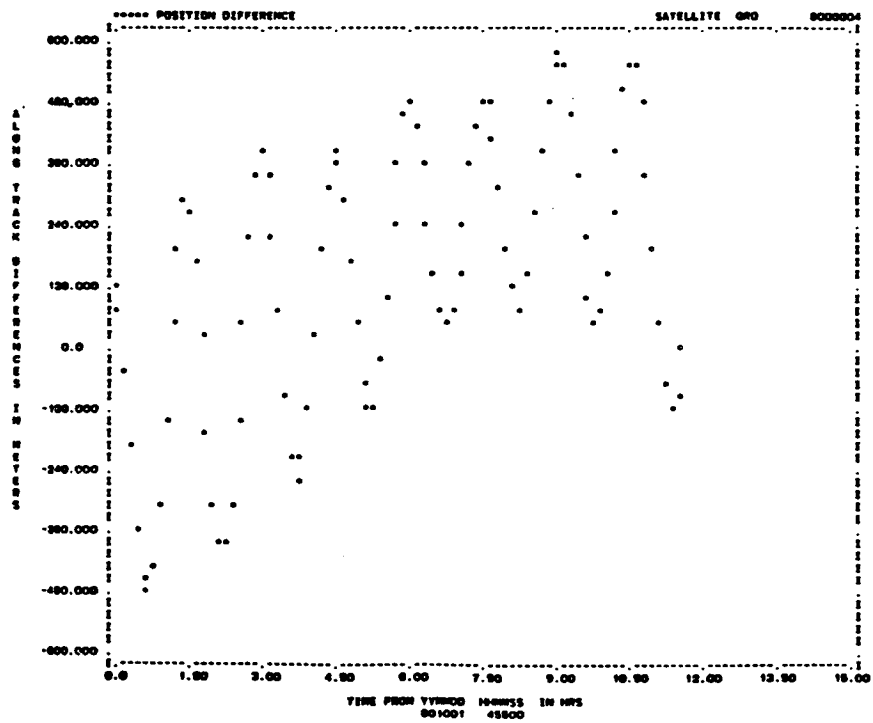


b. 12 to 24 Hours

Figure 5-12. Along-Track Errors for EKF Run T3



a. Second Span



b. Fourth Span

Figure 5-13. Along-Track Errors for SBDC Run G19